

Imperial College London

Department of Electrical and Electronic Engineering

Final Year Project Report 2017

---



Project Title: **A mini-PCB for Glucose-sensor readout and diagnostics**

Student: **Wei Cong Te**

CID: **00831276**

Course: **EEE4**

Project Supervisor: **Dr Sara S. Ghoreishizadeh**

Second Marker: **Professor Christofer Toumazou**

# Declaration of Authorship

I, Wei Cong Te, declare that this thesis titled, 'A mini-PCB for Glucose-sensor readout and diagnostics' and the work presented in it are my own. I confirm that:

- This work was done wholly or mainly while in candidature for a MEng degree at this University.
- Where any part of this thesis has previously been submitted for a degree or any other qualification at this University or any other institution, this has been clearly stated.
- Where I have consulted the published work of others, this is always clearly attributed.
- Where I have quoted from the work of others, the source is always given. With the exception of such quotations, this thesis is entirely my own work.
- I have acknowledged all main sources of help.



# *Abstract*

The project concerns the research and design of a portable mini-Printed Circuit Board (PCB) to perform measurements of metabolite(s) such as glucose with the corresponding three-electrode electrochemical cell. These measurements are then wirelessly sent to a computer or smartphone/tablet. The main focus of this project is to implement features which can potentially supplement the core measurement, such as measuring the impedance of the cell via Electrochemical Impedance Spectroscopy (EIS) as well as cyclic voltammetry. In addition, background subtraction methods such as polynomial fitting and linear estimation are discussed to estimate the metabolite concentration from the cyclic voltammogram. These features are implemented under the constraint that the system is to be battery-powered. The EIS is to be performed over as wide a range of frequencies as possible (ideally DC to 1MHz). Based on currently existing commercial components, it was found that the maximum possible frequency is 100kHz while the minimum is indeed DC. This is due to the aforementioned constraint of being battery powered. Cyclic voltammetry is restricted only to the slow voltage scan variety, with minimum voltage step size of  $100\mu V$  which exceeds the requirement of 5mV steps. The final PCB is fully autonomous and estimated to have a battery life of about 20 days.

# *Acknowledgements*

I would like to express my very great appreciation and thanks to my supervisor Dr Sara S. Ghoreishizadeh for her guidance, patience and care throughout the 9 month duration of this project for the ...

I am particularly grateful for the support and good times given by my friends Mr Daryl Ma, Mr Andrea Mifsud who guided me through Altium and PCB design. Also for all the times we spent working in the lab. Thank you. for...

Finally, to my family, for the care and support throughout my life, especially so throughout the course of my degree.

# Contents

<b>Declaration of Authorship</b>	<b>i</b>
<b>Abstract</b>	<b>ii</b>
<b>Acknowledgements</b>	<b>iii</b>
<b>List of Figures</b>	<b>vi</b>
<b>List of Tables</b>	<b>viii</b>
<b>Abbreviations</b>	<b>ix</b>
<b>1 Introduction</b>	<b>1</b>
1.1 Medical Applications . . . . .	1
<b>2 Project Specifications and Evaluation</b>	<b>3</b>
2.1 Hardware and software specifications . . . . .	3
2.2 Research and Technical Problem . . . . .	5
<b>3 Background</b>	<b>8</b>
3.1 Electrochemical Detection . . . . .	8
3.2 Background Subtraction . . . . .	11
3.2.1 Selection of Background Subtraction method . . . . .	11
<b>4 PCB and Software Design</b>	<b>18</b>
4.1 Overall Block Diagram . . . . .	18
4.2 Hardware . . . . .	20
4.2.1 Data Transmission . . . . .	20
4.2.2 Microcontroller Unit . . . . .	22
4.2.3 Potentiostat and current reading . . . . .	26
4.2.4 Analog-to-Digital Converter . . . . .	29
4.2.5 Impedance measurement . . . . .	32
4.2.6 Programmable Clock . . . . .	42
4.2.7 Custom AFE for impedance measurement . . . . .	44

---

4.2.8	DAC and Analog Switch . . . . .	48
4.2.9	Batteries . . . . .	49
4.2.10	Recharging IC . . . . .	53
4.2.11	Final Hardware Implementation . . . . .	55
4.3	Software . . . . .	57
4.3.1	Software on the MCU . . . . .	57
4.3.2	Receiving End Software . . . . .	66
<b>5</b>	<b>Evaluation and Conclusion</b>	<b>67</b>
5.1	Evaluation . . . . .	67
5.2	Future Work . . . . .	71
5.3	Conclusion . . . . .	73
<b>A</b>	<b>Altium Schematic and PCB layout</b>	<b>74</b>

# List of Figures

2.1	Sensitivity change over time in glucose sensors diagram . . . . .	5
2.2	Sensor current over time diagram . . . . .	5
3.1	Cyclic Voltammogram . . . . .	9
3.2	Amperometry Diagram . . . . .	10
3.3	Potentiostat Configurations . . . . .	10
3.4	Proposed Background Subtraction Diagram . . . . .	13
3.5	Polynomial Fitting Diagram . . . . .	16
4.1	Block Diagram . . . . .	19
4.2	Removal of Quantisation Error with low resolution ADC . . . . .	27
4.3	Analog Subtraction Circuit Diagram . . . . .	27
4.4	Glucose Sensor Equivalent Model . . . . .	34
4.5	PSPICE AFE Simulation . . . . .	35
4.6	PSPICE Data . . . . .	35
4.7	Chronoamperometry of CGMS Sensor . . . . .	36
4.8	EIS of CGMS Sensor . . . . .	37
4.9	AD5933 Simplified Block Diagram . . . . .	37
4.10	Recommended clock frequencies for AD5933 . . . . .	43
4.11	Alternative Potentiostat Configuration . . . . .	46
4.12	Equation for TIA . . . . .	47
4.13	NiMH Discharge Graph . . . . .	51
4.14	LiPo Discharge Graph . . . . .	52
4.15	Final Block Diagram . . . . .	55
4.16	PCB without components . . . . .	56
4.17	PCB with components . . . . .	57
4.18	Complete PCB with Sparkfun breakout board . . . . .	58
4.19	Arduino IDE . . . . .	59
4.20	Serial Communication tool to aid in debugging . . . . .	60
4.21	BLE Polling . . . . .	61
4.22	Main Loop in Code . . . . .	62
4.23	NiMH Discharge Graph . . . . .	63
4.24	NiMH Discharge Graph . . . . .	64
4.25	NiMH Discharge Graph . . . . .	65
5.1	Picture of Prototype . . . . .	68

---

5.2	Picture of prototype with PC, oscilloscope and power supply . . . . .	68
5.3	Picture of new glucose sensor . . . . .	69
5.4	Readings from new sensor . . . . .	70
5.5	Readings from Cyclic Voltammetry . . . . .	70
5.6	Readings from Amperometry . . . . .	71
5.7	Readings from EIS . . . . .	72
A.1	Microcontroller Schematic . . . . .	74
A.2	Battery Charging Schematic . . . . .	75
A.3	AFE Schematic . . . . .	75
A.4	AD5933 Impedance Analyser Schematic . . . . .	76
A.5	PCB Layout . . . . .	76
A.6	3D view of PCB . . . . .	77

# List of Tables

3.1	Background Subtraction methods table . . . . .	17
4.1	Data Transmission IC table . . . . .	22
4.2	Table of Microcontroller . . . . .	23
4.3	Potentiostat AFE comparison table . . . . .	28
4.4	Comparison of low-power ADCs . . . . .	30
4.5	Impedance measuring AFE table . . . . .	38
4.6	Table of Waveform Generators . . . . .	39
4.7	Table of high speed ADCs . . . . .	40
4.8	Table of Programmable Clock ICs . . . . .	43
4.9	Table of Op-Amps . . . . .	46
4.10	Table of DAC . . . . .	49
4.11	Table1 of Batteries . . . . .	50
4.12	Table2 of Batteries . . . . .	50
4.13	Table of charger ICs . . . . .	53
4.14	Summary of PCB Capabilities . . . . .	55
4.15	Table of BLE commands . . . . .	59

# Abbreviations

<b>AC</b>	<b>A</b> lternating <b>C</b> urrent
<b>AFE</b>	<b>A</b> nalog <b>F</b> ront <b>E</b> nd
<b>DC</b>	<b>D</b> irect <b>C</b> urrent
<b>DSP</b>	<b>D</b> igital <b>S</b> ignal <b>P</b> rocessor
<b>PCB</b>	<b>P</b> rinted <b>C</b> ircuit <b>B</b> oard
<b>FPU</b>	<b>F</b> loating- <b>P</b> oint <b>U</b> nit
<b>NiMH</b>	<b>N</b> ickel- <b>M</b> etal <b>H</b> ydride
<b>LiPo</b>	<b>L</b> ithium <b>P</b> olymer
<b>SMD</b>	<b>S</b> urface <b>M</b> ount <b>D</b> evice
<b>EIS</b>	<b>E</b> lectrochemical <b>I</b> mpedance <b>S</b> pectroscopy
<b>CE</b>	<b>C</b> ounter <b>E</b> lectrode
<b>RE</b>	<b>R</b> eference <b>E</b> lectrode
<b>WE</b>	<b>W</b> orking <b>E</b> lectrode
<b>GUI</b>	<b>G</b> raphical <b>U</b> ser <b>I</b> nterface
<b>BS</b>	<b>B</b> ackground <b>S</b> ubtraction
<b>redox</b>	<b>r</b> eduction- <b>o</b> xidation reaction
<b>GOx</b>	<b>G</b> lucose <b>O</b> xidase <b>E</b> nzyme
<b>op-amp</b>	<b>O</b> perational <b>a</b> mplifier
<b>ADC</b>	<b>A</b> nalog-to- <b>D</b> igital <b>C</b> onverter
<b>DAC</b>	<b>D</b> igital-to- <b>A</b> nalog <b>C</b> onverter
<b>AFE</b>	<b>A</b> nalog <b>F</b> ront- <b>E</b> nd
<b>sps</b>	samples <b>p</b> er <b>s</b> econd
<b>TIA</b>	<b>T</b> ransimpedance <b>A</b> mplifier
<b>DFT</b>	<b>D</b> iscrete <b>F</b> ourier <b>T</b> ransform



<b>IC</b>	<b>I</b> ntegrated <b>C</b> ircuit
<b>USB</b>	<b>U</b> niversal <b>S</b> erial <b>B</b> us
<b>BLE</b>	<b>B</b> luetooth <b>L</b> ow <b>E</b> nergy
<b>MCU</b>	<b>M</b> icro <b>C</b> ontroller <b>U</b> nit

# Chapter 1

## Introduction

This project aims to build a miniature printed circuit board (PCB) which will interface some biosensor(s) and be able to periodically obtain an accurate reading from the sensor(s) and send the data to a computer or a mobile phone. These sensors are typically three-electrode electrochemical cells. In addition to this, it should be able to provide some extra information about the sensor such as the cell impedance which will allow the PCB to self-calibrate the sensor readings. This is as compared to the user performing manual calibration which is the case for commercial glucometers, be it single-use finger sticks or continuous glucose monitoring. This report will discuss the project specifications and technical challenges in Chapter 2, the background regarding electrochemical sensing and the main focus of this project which is background subtraction in Chapter 3, the overall hardware and software design in Chapter 4 and finally the evaluation and conclusion in Chapter 5.

### 1.1 Medical Applications

The main motivation for obtaining precise and accurate readings from biosensors is that they are used to detect various metabolites. The importance of this is that these metabolites are used to either detect or treat medical conditions. Of the endogenous metabolites that exist, the most interesting[1] are: glucose (treatment of diabetes)[2], cholesterol (detection of various diseases such as anemia and

atherosclerosis and more)[3], lactate (sports medicine and detecting patient oxygen supply for use in special care units)[4] and glutamate (detection and treatment of myocardial and hepatic disease)[5].

The added benefit of having biosensors collecting data from every individual is the potential for personalised medicine[6], which will allow doctors to customise the treatment to the patient. One example where this will prove useful is in the treatment of rheumatoid arthritis. For this disease, a significant proportion of patients do not respond to expensive but generic treatment which may be effective for the other patients[7].

This makes having an integrated, multi-purpose detection platform which will work with different sensors for different metabolites very attractive.

# Chapter 2

## Project Specifications and Evaluation

### 2.1 Hardware and software specifications

This project aims that a handheld device capable of measuring multiple metabolites (such as glucose, lactate and glutamate) be designed and made. In general, the PCB will be made to handle continuous monitoring, such as that for continuous glucose monitoring. In this scenario, the PCB is always supplying a constant DC voltage to the sensor such that the correct cell voltage is applied across the working electrode and reference electrode. However, it can be reasonably assumed that the device can be reprogrammed to perform sensing on demand, for example with glucose finger sticks.

The formal requirements are to create a sensing tag for diabetes management through design, implementation and test of a mini-PCB (small enough to be portable, for example, approximately the size of a modern smartphone or smaller). Ideally, the PCB must be capable of:

1. Measuring sensor current (within 10nA to 50 $\mu$ A)
2. Measuring sensor impedance (from DC to 1MHz)
3. Capable of taking impedance values and applying algorithms to determine sensor sensitivity

4. **Real-time background current correction** (Main challenge of project and will be elaborated upon in the next section)
5. Battery-powered and can last one week before recharging through smart activity programming
6. RFID/NFC bi-directional communication to a laptop/tablet/smartphone for further processing and display
7. Bonus: Recharging via NFC/RFID or being powered purely through NFC/RFID without a battery

Do note that the algorithms relating impedance to sensitivity are still being developed externally to this project and are not actually implemented in this project. However, the device should be capable of being reprogrammed to do this in the future. It is also worth noting that an attempt was made to characterise this change in sensitivity using the complex impedance of the sensor via electrochemical impedance spectroscopy by Zhang[8]. Zhang's thesis directly influences the requirements for measuring sensor impedance and as such, complex impedance and some way to implement a 1024-point discrete fourier transform (DFT) are required since these are what Zhang uses to correlate impedance and sensitivity[8].

In terms of impedance range, while it is not explicitly specified, a reference to Zhang's thesis gives an indication that the complex impedance for the glucose sensor ranges from low hundreds to over  $1000\Omega$  and therefore the range that will be targeted is  $100\Omega$  to  $2000\Omega$ .

For sensor current, it has been deemed that the minimum resolution required is three times smaller than the minimum current and so the PCB should be able to distinguish between current differences of  $3nA$ .

In addition to hardware requirements, software must be developed to interface the PCB. The requirement is that data be able to be viewed on a phone or on MATLAB. This allows for easy viewing and data processing.

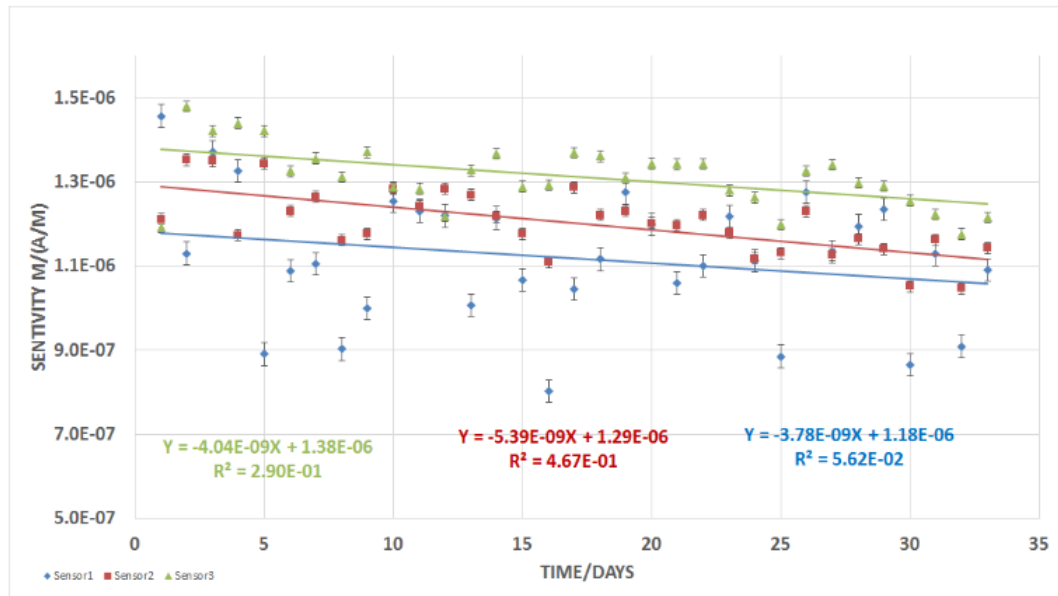


FIGURE 2.1: Change in sensitivity over time for three glucose sensors of the same brand and model[8]

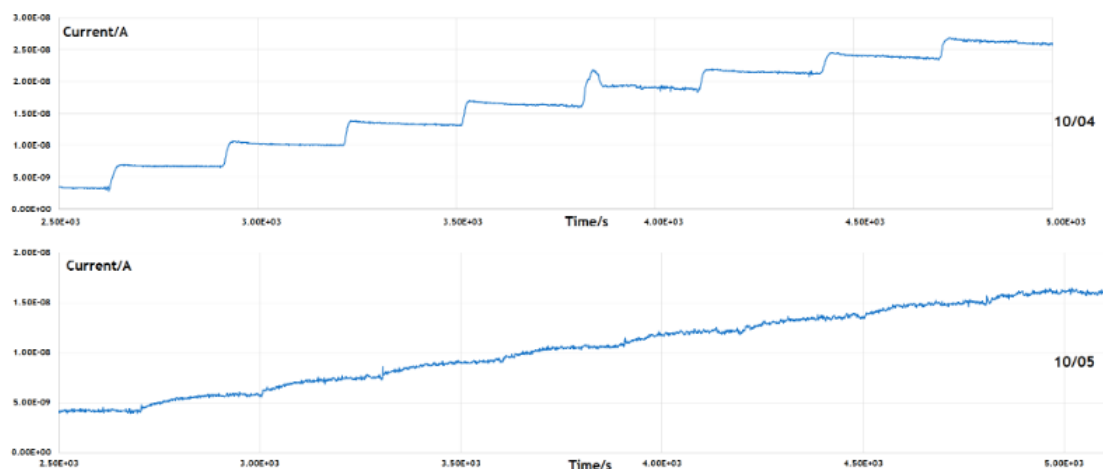


FIGURE 2.2: Difference in current for the same concentration of glucose over 2 consecutive days[8]

## 2.2 Research and Technical Problem

As stated, the main focus of this project is to interface with bio-sensors. There are two issues with today's commercially available bio-sensors. These 2 issues also form the main challenges of this project.

The first problem is that they require constant calibration from the user. In the context of glucose sensors, this is due to their unpredictable change in sensitivity over time[8] as can be seen in Figure 2.1. This makes it difficult to determine the

exact concentration of glucose given a certain current as can be seen in Figure 2.2, where the output currents are drastically different on 2 consecutive days. This makes it difficult to simply compute current sensitivity based on historical sensitivity. This project aims to capitalise on Zhang's efforts and calculate the sensor's sensitivity automatically, without the need for the user to perform the calibration. Therefore, a fast and low-power method of obtaining the impedance of the sensor must be incorporated into the PCB.

The biggest technical challenge that arises from impedance measurement is the high frequency of 1MHz required. This necessitates the use of analog to digital converters (ADCs) which sample at a minimum 2 million samples per second (MSPS) according to the Nyquist theorem. This means that the receiving controller, be it a microcontroller or DSP, has to be able to read the data at a minimum of  $2MSPS * bits\ per\ sample$  on a serial interface (which is one of the most commonly used interface). This is not a trivial problem when considering that the device has to be portable and battery powered, not run off bench power supplies or wall sockets. This challenge will be discussed in greater detail in Chapter 4 when the design decisions regarding the PCB is presented.

The second problem is that metabolite measurement done via amperometry or cyclic voltammetry can constitute a large background current with a small signal current (in general on the scale of nA with the background being one or two orders of magnitude higher), the sum of which is directly measured from the sensor. Since the aim of this device is to eliminate the need for user calibration, the background current cannot be directly measured. This makes sense given that human blood always contains some non-zero amount of metabolite, for example glucose or cholesterol.

However, estimating this background is not trivial. As Zhang shows in his thesis, the impedance of a glucose sensor varies wildly and in an irregular fashion, similar to its sensitivity[8]. This means that even with no glucose in the solution, the current readings will vary wildly for the same voltage applied across the electrochemical cell of the sensor. Despite this, this project aims to apply some form of background subtraction (BS) to filter out the background and obtain only the signal current. Note that this background subtraction will work for any generic metabolite given the respective sensor. The only difference will be the reduction-oxidation reaction (redox) voltage associated with different chemicals. This will be explained in further detail in the next chapter.

---

Finally, as a note, please do be aware that the rest of this paper will be discussing the problem in the context of glucose sensors due to the problems highlighted above. But, this does not take away from the multiple metabolite sensing as long as amperometry or cyclic voltammetry is used to detect the metabolites since the voltage of the cell and the voltage sweep can be changed in software to suit a particular metabolite.



# Chapter 3

## Background

### 3.1 Electrochemical Detection

Fundamentally, the PCB will be designed to work with electrochemical sensors. Specifically, these sensors will make use of cyclic voltammetry or amperometry to measure the amount of metabolite present. Cyclic voltammetry is the process whereby the potential between the working electrode and reference electrode in an electrochemical cell (also known as cell potential) is swept in a linear ramp as can be seen in Figure 3.1. For the application of sensing certain metabolites such as glucose, the cyclic voltammetry will be slow (as stated in the specifications, 30 to 300mV/s as opposed to fast-scan such as 300 to 400V/s for dopamine[9][10][11], a neurotransmitter). Cyclic voltammetry has to be done repeatedly over a period of many minutes to an hour in order for the sensor to stabilise [6], otherwise the sensor will be giving false readings. The current is measured and then plotted against the input voltage, and this is also shown in the same figure. This resultant plot is known as a voltammogram. Peak detection will be performed on the output and these peak voltages will give an indication of what metabolites exist in the sample solution based on existing knowledge of redox reactions and their respective voltages. The amplitude of each peak is then proportional to the concentration of metabolite.

Take note however, that this does not necessarily mean that the metabolite is directly involved in the redox. In the case of glucose, detection is usually done by introducing an enzyme called glucose oxidase (GOx). An enzyme is a biological substance which acts as a catalyst to increase the rate of a biochemical reaction

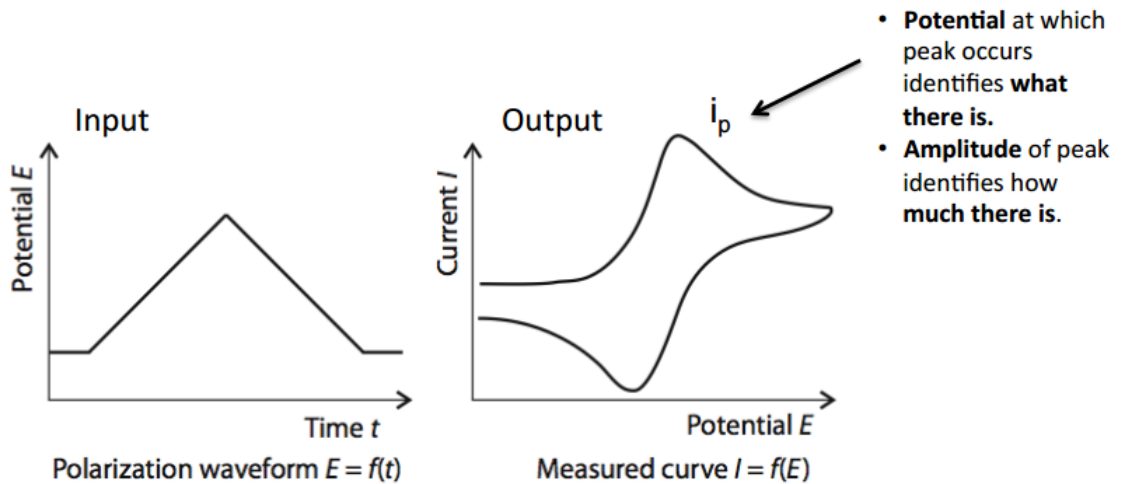
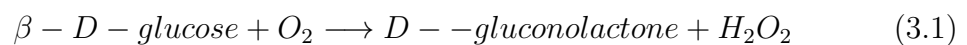


FIGURE 3.1: Cyclic Voltammetry and the resulting voltammogram[12]

which is specific to that enzyme. In living organisms, it is critical for metabolism, which would be extremely slow otherwise[13]. In the case of GOx, it catalyses the oxidation of beta-D-glucose (which is found in human blood) into D-gluconolactone and hydrogen peroxide[14] as shown in Equation 3.1. Redox of hydrogen peroxide into water and oxygen when 0.7V is applied across the electrochemical cell is what is finally measured and the chemical equation is seen in Equation 3.2. Since hydrogen peroxide does not normally exist in blood, this redox and the current generated from it will give an indication of the concentration of glucose present. Similar reactions exist for the other endogenous metabolites such as lactate oxidase enzyme with lactate[1].



Amperometry can be seen as voltammetry at a fixed, constant voltage over time, and is also called chronoamperometry. As before, the sensor will be driven for some time to ensure the sensor is stable before current is measured. The difference is, the current is now plotted against time and is called an amperogram, as shown in Figure 3.2, where the current is measured for different concentrations of glucose. Amperometry is done when only one specific metabolite is of interest, and the test is conducted to only detect that metabolite.

Finally, a potentiostat is usually used to drive the electrochemical cell and maintain the potential across the working electrode and reference electrode, be it constant

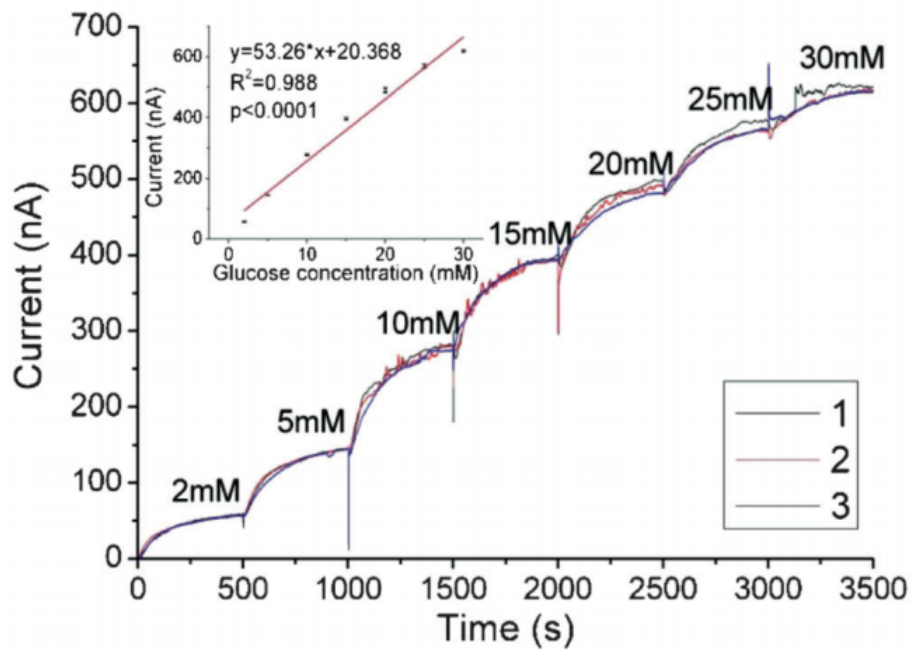
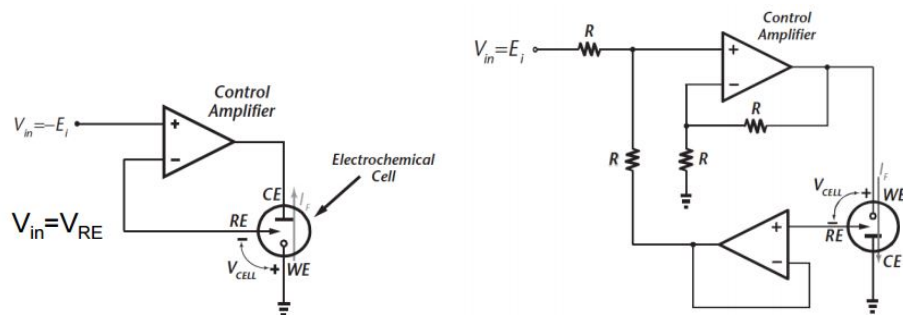


FIGURE 3.2: Chronoamperometry of glucose[12]



(A) Grounded working electrode (B) Grounded control electrode configuration[12]

FIGURE 3.3: Two common potentiostat configurations

or voltage sweep. There are several common configurations possible, either a grounded working electrode configuration (shown in Figure 3.3a) or a grounded counter electrode (shown in Figure 3.3b). There are other configurations which are variations of these two configurations but in general one or more operational amplifier (op-amp) are used to drive the cell.

## 3.2 Background Subtraction

The main challenge of this project is the background subtraction. Background subtraction (BS) is commonly used in image processing and computer vision to detect movement in video[15], since what is of interest is the moving object and not the static background. While this project does not involve any image processing, the general principle of retrieving a signal against a background is the same. Many of the techniques used in BS for computer vision follow a general scheme[16] which is applicable to this project as well:

1. Background Initialisation
2. Foreground Detection
3. Background Maintenance

Background initialisation refers to building a model of the background using a fixed number of frames (or in this case, using some initial current measurements). Foreground detection refers to detecting the differences between new data and the background model; in general subtraction is done to detect said differences and therefore extract the signal. Finally, background maintenance refers to updating the background model over time with a learning algorithm that has a learning rate.

For the purposes of this project, this broad outline fits the requirements very well. The background (sensor current in the complete absence of metabolite) has to be estimated using a model. The exact model to be used will be discussed later in this chapter. The extra current due to the presence of the metabolite will be extracted using Foreground Detection and finally due to the constantly changing impedance of the sensor (especially for glucose sensors), the background model has to be constantly updated as well with Background Maintenance.

### 3.2.1 Selection of Background Subtraction method

Of course, the specific techniques used in computer vision such as Kalman Filtering will not fit the purposes of this project. The techniques used to detect background current can come in the form of direct measurement, eliminating altogether the

need for a background model in background initialisation. This is used in applications such as dopamine detection, where fast-scan cyclic voltammetry (rapid voltage sweep, on the order of few hundred to thousands of  $V/s$ ) is carried out due to the subsecond resolution required in testing for dopamine release due to stimuli or drug responses[10]. In that application, it is possible to obtain a baseline in the complete absence of stimuli. The measured background is then subtracted from subsequent measurements, under the assumption that the background does not significantly change for subsequent measurements. This has in fact been done by Alyssa B. Apsel et al.[17]. In fact, the team assumed that the background did not significantly drift over a period of 40 seconds which meant that the background need only be captured every 40 seconds and this view is supported by Wightman[9] and Robinson[10], both of which essentially state that the background is stable over seconds but not over minutes.

This method however, was deemed unsuitable due to the way it establishes relative levels (stimuli vs no stimuli) and does not give absolute values. To get absolute values, measurements must be made in the absence of or a known level of metabolite. One way to do it might have been to perform calibration with standard test solutions on the glucose sensor every time before use, thereby establishing the background model directly. But this contradicts with the objective of this project, which is to make a calibration-free method of detecting metabolites.

The alternative would be to incorporate a background model with an initial measurement. The baseline is measured once before the use of a sensor, and thereafter background maintenance can be done by updating the background model according to either a function of time or actual impedance measurements through the PCB. This function of time would model how the glucose sensor degrades with respect to time. However, as explained previously, the impedance of the sensor constantly changes in an erratic fashion, making modelling extremely difficult and hence making this method intractable. As for impedance measurements, it is worth noting that cyclic voltammetry voltage-current curves distort in shape over time. This is due to degradation of the glucose sensor over time and also changes in concentration of other chemicals in blood that are picked up in the voltammetry. This makes pure impedance measurements insufficient to characterise the voltammetry curve.

Other methods include using a second sensor which is always connected to a reference solution with a known amount of glucose[18] as proposed by Jonathon O.

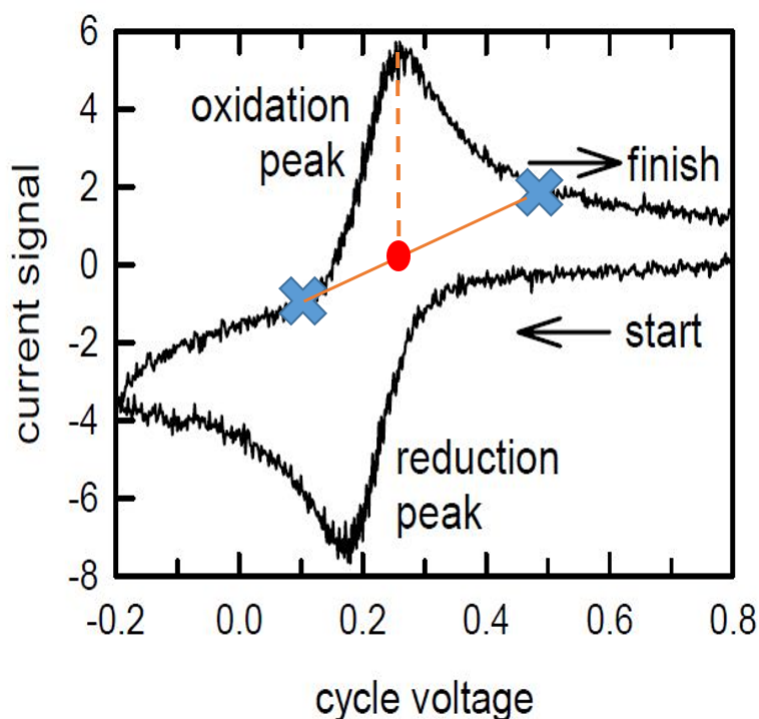


FIGURE 3.4: Proposed method of background subtraction

Howell et al. However, as Zhang shows in his research, two sensors of the same brand and model do not change similarly over time in terms of both impedance and sensitivity as shown in Figure 2.1, rendering this method ineffective.

Another method proposed by Paula S. Cahill et al. is analog filtering[19], where by the driving signal into the cell is high pass filtered. This is done in fast-scan cyclic voltammetry to reduce background current. However, this is ineffective in slow cyclic voltammetry like that which is done for glucose (about 30 to 300mV/s and one cycle can take half an hour to complete) since the voltage sweep is of an extremely low frequency, and making high pass analog filters for very low frequencies is very difficult.

Therefore, a method inspired by background detection was devised. Since it is too difficult to characterise the voltammogram curve and calibration/comparing against a reference solution is out of the question, the next best method is to perform partial background removal via linear estimation as the background model. This is shown in Figure 3.4. Note that this figure is not drawn to scale and is exaggerated to make the explanation clear. In reality, the redox peak is small relative to the magnitude of the current measured in the voltammogram.

The assumption here is that the cyclic voltammetry will not be carried out in the presence of multiple metabolites, each of which has a peak at different voltages. Or that at the very least, the peak voltages are sufficiently different that the base of the peaks (marked in crosses in Figure 3.4) are spaced apart in the voltammetry graph. The voltammetry shown in Figure 3.4 has only one clear peak. This simplifies the explanation but the same principle can be applied to multiple peaks, as long as the assumption above holds. Linear estimation is shown here as estimating the background current based on taking a linear approximation, ideally by taking 2 actual current readings at the base of the peaks. A linear estimation of the form  $Current = m \cdot Voltage + c$  will be performed, using the actual current readings to determine the parameters  $m$  and  $c$ . In this way, the background is estimated at the voltage level where the peak exists (shown as a red dot in Figure 3.4).

A linear estimation is not very sophisticated, but it has the advantage of being cheap to perform and can be done locally on the PCB without consuming large amounts of power which will adversely affect the battery life goals of this project. The accuracy of linear estimation will have to be determined using actual voltammograms for a variety of sensors, ones where the glucose level is known and therefore the estimate can be compared against it. The best commercial glucometers have average errors between 5.5% to 7%, with the worst having error rates greater than 8.5%[\[20\]](#). If linear estimation is found to be comparable to the commercial sensors, it will be deemed a suitable method of BS. Work can then be carried out to characterise different commonly used sensors to determine experimentally at what voltage does the peak occur and at what voltages do the bases of the peak reside.

Alternatively, should linear estimation prove to be too inaccurate, alternative curve fitting methods such as iterative polynomial fitting will work as shown by Jakubowska et al.[\[21\]](#) who applied it to the context of voltammograms (although none of which have really small peaks). The exact method has yet to be determined but a good starting point will be that as described by Gan et al.[\[22\]](#). As Gan describes, polynomial fitting is fitting a equation of the form:

$$y(x) = a_0 + a_1x + a_2x^2 + \dots + a_nx^n \tag{3.3}$$

For a set of  $x$  values  $x_1, x_2, x_3, \dots, x_m$  we can write the following matrix:

$$\begin{bmatrix} y(x_1) \\ y(x_2) \\ y(x_3) \\ \dots \\ y(x_m) \end{bmatrix} = \begin{bmatrix} 1 & x_1 & x_1^2 & \dots & x_1^n \\ 1 & x_2 & x_2^2 & \dots & x_2^n \\ 1 & x_3 & x_3^2 & \dots & x_3^n \\ \dots & \dots & \dots & \dots & \dots \\ 1 & x_m & x_m^2 & \dots & x_m^n \end{bmatrix} \begin{bmatrix} a_0 \\ a_1 \\ a_2 \\ \dots \\ a_n \end{bmatrix} \quad (3.4)$$

This can be written as the compact matrix equation:

$$\mathbf{y} = \mathbf{X}\mathbf{a} \quad (3.5)$$

And so the polynomial fitting should give us a result such that:

$$\hat{\mathbf{b}} = \mathbf{X}(\mathbf{X}^T\mathbf{X})^{-1}\mathbf{X}^T\mathbf{y} \quad (3.6)$$

Where  $\hat{\mathbf{b}}$  is the estimate of  $\mathbf{y}$  and  $^T$  and  $^{-1}$  refers to the transpose and inverse of a matrix respectively. In this application, the exact parameters of  $\mathbf{a}$  can be determined iteratively as long as the order of the polynomial is decided. It is shown by Jakubowska that the optimal fitting is between 2<sup>nd</sup> to 6<sup>th</sup> order polynomials and the exact order will have to be determined experimentally based on the sensor.

As for the algorithm, the idea is upon every iteration, all data points in  $\mathbf{x}$  which are larger than the estimate will be replaced by the estimate and the fitting done again. This is done up a few times to get a flattened shape with no peaks which approximate the background current. This is illustrated in Figure 3.5.

The drawback of this method is that matrix multiplication is expensive and this is unlikely to be implemented on a low power microcontroller which will be used on the PCB. If this method is chosen, then it is likely that the implementation will be done on the receiving device.

Finally, the following table summarises methods of background subtraction that has been presented so far:



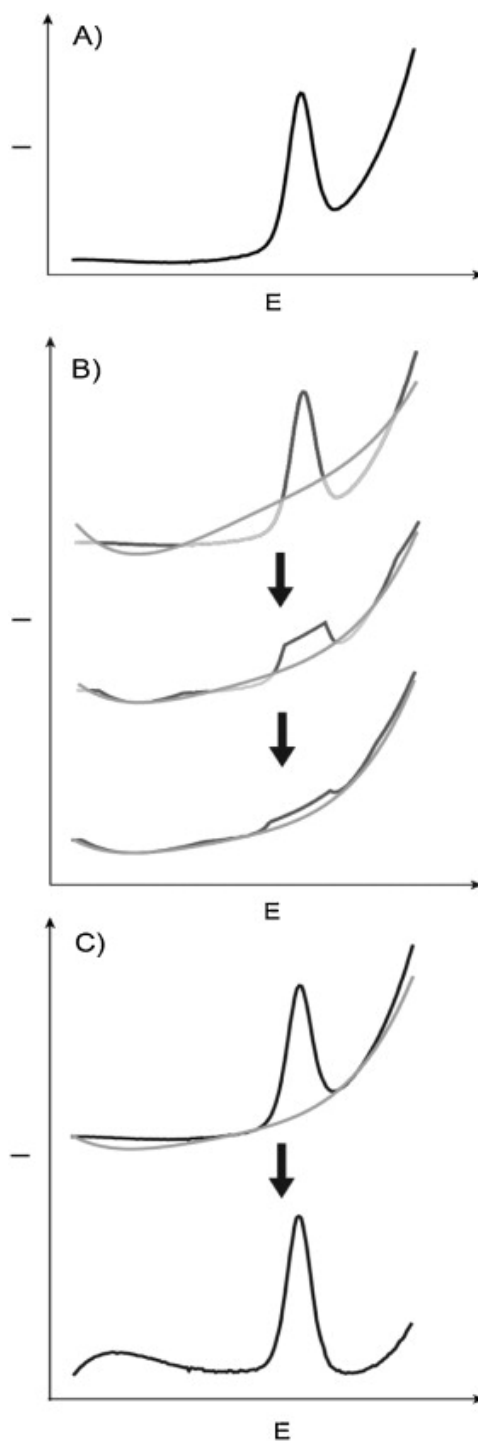


FIGURE 3.5: Alternative method: polynomial fitting[21]

Property/Method and Author	Analog Background Subtraction, Alyssa[17]	Offset Compensation, Howell[18]	Analog Filtering, Cahill[19]	Linear Estimation, Wei	Polynomial Fitting, Jakubowska[21]	Possible/Desirable for this project
Uses direct measurement of background	Yes	Yes	No	No	No	Not possible when metabolites always exist in blood
Uses 2 cells, one with reference and one for actual measurement	No	Yes	No	No	No	Undesirable, since 2 similar sensors change sensitivity differently from one another
High pass filtering	No	No	Yes	No	No	Not possible, too low main frequency in voltammetry
Simple computation for microcontroller	Yes	Yes	Yes	Yes	No	Desirable, especially if a mobile app is to be developed but not a must
Correction for quantisation error	Yes	No	No	No (but can be included)	No (but can be included)	Desirable, because this allows a lower power, fewer bits ADC
Shown to work in peer reviewed articles	Yes	Yes	Yes	No	Yes	Desirable but not a must as results can be obtained during testing
Core method can be applied to this project	No	Yes, if errors caused by impedance and sensitivity mismatch is low and tolerable	No	Yes	Yes	Desirable, a must

TABLE 3.1: Table of Background subtraction methods

# Chapter 4

## PCB and Software Design

### 4.1 Overall Block Diagram

One method of getting very precise, low noise and fast measurements that have been implemented by Papadimitriou et al. is to use a field-programmable gate array (FPGA)[23]. This allows for on-board digital signal processing (DSP) units to perform fast DFTs which is desirable in this project and the ability to easily monitor multiple bio-sensors which is a bonus but not a requirement. The team used a commercial Xilinx Spartan3e FPGA and are able to detect input current from tens of pA up to hundreds of  $\mu\text{A}$  and input voltages from hundreds of  $\mu\text{V}$  to hundreds of mV with good, consistent linearity in testing[23]. However, whilst it is not mentioned in the paper how much power it consumes (the team runs it off a 220V, 50Hz AC supply[23]), the use of high-precision, high speed Digital-to-Analog Converters (DAC) and Analog-to-Digital Converters (ADC) in addition to a commercial FPGA. Based on published research that have measured power consumption of FPGAs for particular applications, it is found that FPGAs have power consumptions in tens of mW to a few W[24][25][26][27]. This leads to the reasonable conclusion that this method is too power hungry for this project's purpose of making a device that will last 7 days on a single charge.

Therefore, the traditional method of using a simple, low power microcontroller unit (MCU) based system was chosen, with the criteria for a simple DSP being set as "good to have, but not a must". The reason for this is that the DFT can be performed on the receiving device such as a laptop (whose power consumption is out of the scope of this project), at the cost of sending more data points

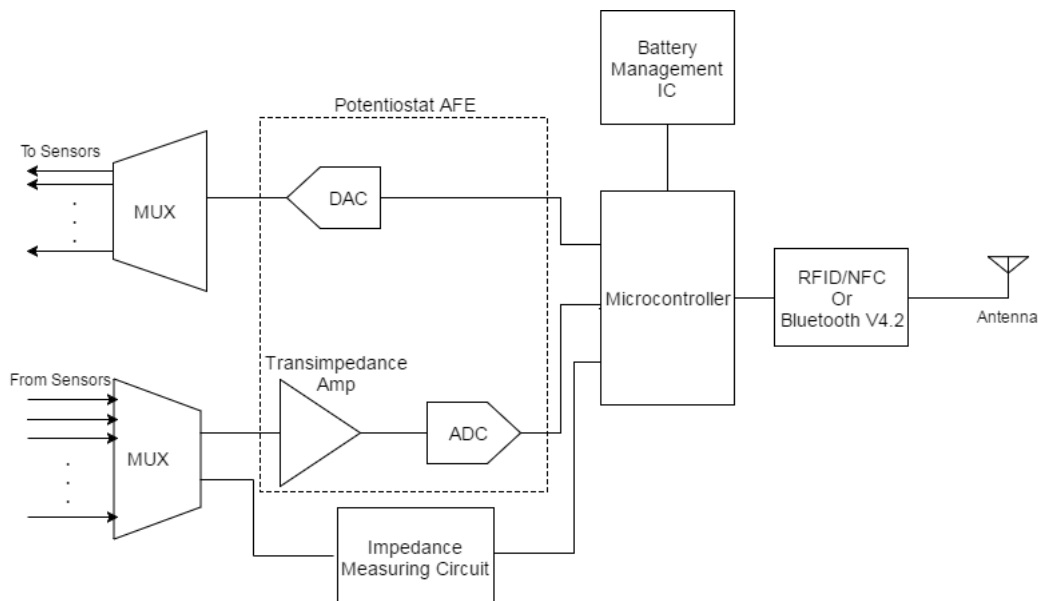


FIGURE 4.1: Initial block diagram of proposed PCB

to the laptop as opposed to just sending the real and imaginary components of impedance.

The key blocks for the PCB have been identified as shown in Figure 4.1. These will handle what the PCB is required to do, which is to drive an electrochemical cell, take current and impedance measurements and send these readings wirelessly to an external receiver. It is noted that for slow-scan cyclic voltammetry, the components required are identical to amperometry except that the DAC needs to be periodically updated with the next voltage value. Since the DAC is not refreshed at a high rate, it is assumed for now that the bandwidth of the amplifiers and sampling rates of the ADC used in chronoamperometry are sufficient. This will be examined in detail later in this section when the hardware is discussed. Note that the final block diagram will be shown in the final part of the hardware section.

## 4.2 Hardware

First and foremost, the device must be able to be powered by just batteries. Therefore, the hardware design is designed around the core tenet of low power. In other words, the specifications laid out in Chapter 2 will be secondary and trade-offs in reduced capability for reduced energy consumption will be made where necessary.

Secondly, the PCB needs to be small and portable. Therefore, there is also a aim to keep the number of components down, to reduce the total footprint and therefore PCB size required.

### 4.2.1 Data Transmission

The first thing that was considered was data transmission. The data transmission system should be robust and consume as little power as possible, with no need for high data rates due to the fact that it is perfectly reasonable for the sensor data or phone commands to the PCB to arrive seconds later instead of a few milliseconds. Should the transmission be wireless, it is strongly desirable to be able to obtain off-the-shelf antennas for it. This is as antenna design is extremely complicated and will take too much time from this project to research, design, test and implement an antenna.

Because the target receiving platform is potentially a tablet or smartphone, it would be desirable that the transceivers used in this project are compatible without an extra add-on to the phone. This leaves communications that come as standard on smartphones and tablets. These would be: Wi-Fi, Bluetooth, Near field communication (NFC) and Universal Serial Bus (USB), all of which are standard protocols. Special attention was made to verify that antennas were available for the first three wireless protocols. Indeed, it is found that commercial antennas such as the Abracon AMCA31-2R450G-S1F-T[28] are available for Bluetooth which uses the 2.4GHz band. The same is true of NFC and Wi-Fi such as the Pulse W7001[29] which is tuned for NFC at 13.56MHz and Pulse W3108 for Wi-Fi[30].

Comparing the available options, USB will ensure the most reliable communications since communications happen over a physical cable. However, it is undesirable in this application. This is due to the constant need to have a wire connecting

the device to the PCB which makes the device more cumbersome. NFC also has the same issue of being cumbersome for the user. Despite having very low sleep current ( $\mu\text{A}$  range) and moderate current consumption during transmission (tens of mA range)[31], NFC require that the transmitter and receiver be in very close proximity, usually below 20cm[32]. This makes it easy for the user to forget to obtain updated readings as well as become a hassle. In addition, NFC tend to have low data rates (maximum of 424kpbs and in practice closer to 100kpbs[31]). This makes long data transfers more of an issue, forcing the user to maintain the proximity which can be unpleasant whilst also increasing the chance of corrupt data/incomplete transfers. The PCB can be expected to have long data transfers every time EIS is performed. This is due to the larger data size from the wide frequency range that the PCB measures over. Therefore, NFC was dropped as a potential data transmission technology.

Of the remaining two, it is found that in general, Wi-Fi has the highest throughput and consequently the highest power consumption, both when idle (but connected/paired) and during data transmission/receiving[33]. Unconnected power consumption and Bluetooth advertising power consumption are not considered since it is expected that the PCB will spend a majority of the time being connected to a device. With regards to Bluetooth, there are two variants. Bluetooth version 4.0 and newer feature classic Bluetooth as well as a low energy variant called Bluetooth Low Energy (BLE). BLE trades off data rate (1Mbps vs up to 24Mbps for classic Bluetooth) for lower power consumption (minimum of -20dBm vs 0dBm for classic Bluetooth). 1Mbps is still more than fast enough for this application, especially when the PCB can reliably communicate with the paired device without active user intervention. Therefore BLE was selected over WiFi and classic Bluetooth.

It can be noted that BLE is a relatively new feature which can only be found on more recent smartphones and tablets which limits the PCB's compatibility. However, this is a reasonable choice given the lower power consumption of BLE and NFC compared to traditional Bluetooth protocol which is available on the vast majority of existing phones and tablets. In addition, this PCB is akin to a continuous glucose monitoring system. These systems are quite expensive. The Juvenile Diabetes Research Foundation in the UK give estimates of between £1000 to £2500 upfront cost, with running costs of £40 to £60 for a sensor change every

7 days[34]. It can therefore be reasonably assumed that the users will own a newer smartphone and be able to use this PCB.

There are many transceiver ICs available for BLE, some of which are shown in Table 4.1.

Specifications/IC	SPBTLE-RF	nRF52832	CC2640	PAN1740
Bluetooth Version	V4.1	BLE v4.1	BLE v4.1	BLE v4.0
Supply Voltage (V)	1.7-3.6	1.7-3.6	1.8-3.8	2.35-3.3
Transmit Power (mW)	2.5	0.01-2.51	0.01-3.16	1
Transmit Current (mA)	NIL	5.3 peak	9.1	4.9
Receive Current (mA)	NIL	5.4 peak	5.9	4.9
Supply Current (standby) ( $\mu$ A)	2	1.9	1	5
Data Rate (kbps)	24000	1000 or 2000	1000 or 2000	1000
MCU	None	ARM Cortex M4F	ARM Cortex M3	ARM Cortex M0

TABLE 4.1: Table of BLE ICs

Given that it can be reasonably assumed that the user will have the phone and PCB near them at all times, a high transmit power is not necessary. Priority is given to low current consumption during standby, transmitting and receiving. This narrows down the choice to PAN1740 and nRF52832. The major difference between the two are their paired microcontroller units (MCU). However, this does not completely rule out the use of a second, external MCU and the final choice for both BLE IC and MCU will be presented in the next section when MCUs are examined in more detail.

## 4.2.2 Microcontroller Unit

The MCU should be low-power, but at the same time sufficiently powerful with enough on-board memory to handle BLE, background subtraction and the high data transmission rates from EIS.

From the previous subsection, we can see that BLE chips can come with on-board MCUs which can be used as a general processor on top of coordinating Bluetooth connections. From a power consumption and system complexity point of view, it would be preferred to use one MCU for the entire system rather than have a

Specification/MCU	Cortex M0	Cortex M3	Cortex M4F
Power Consumption ( $\mu$ W/MHz)	16	32	33
Clock Speed (MHz)	16	48	64
DMIPS/MHz	0.84	1.25	1.25
FPU and DSP	No	No	Yes
Flash Memory (kB)	32	128	512
RAM (kB)	42	28	64
Architecture (Bits)	32	32	32
GPIO	12	Up to 31	32
SPI SCLK (MHz)	16	12	8

TABLE 4.2: Table of Microcontroller

separate one to control the board and another to handle the BLE communications. Having a BLE chip with an on-board MCU also removes the burden of having to build our own Bluetooth stack as it is usually pre-loaded onto the MCU. The Bluetooth stack is essentially software which implements the Bluetooth protocol.

As a point of reference, it is common to find commercial BLE chips which are advertised as being low-power being paired with ARM Cortex-M series processors, including the ICs listed previously. This gives a good yardstick of the level of processing power and on-board memory required versus energy consumption. Table 4.2 below shows the M series processors used by the BLE ICs:

Note that the specifications are taken from the BLE ICs. In reality, the Cortex M3 and M4F can run much faster, up to 200MHz. In addition, the amount of flash memory, RAM and GPIO will vary from IC to IC using the same processor. The Cortex M4F is the only MCU which comes integrated with a Floating-Point Unit (FPU) and Digital Signal Processor (DSP). Between the Cortex M3 and M4, there is no real reason to use the Cortex M3. It has a marginally lower power consumption but does not come with the aforementioned FPU and DSP, which can help compute results faster, thereby keeping the Cortex M4 active for a shorter period of time. This directly translates into power savings.

Based on power consumption alone, the Cortex M0 should be ideal since it consumes the least power while active. These power figures are generally not reflected in the previous table of BLE ICs, which are only concerned with power consumption during idle, transmit and receive.

However, the Cortex M0 is deemed to be not powerful enough due to the low clock speed and low DMIPS. More importantly, the BLE IC which it is integrated



into has very little flash memory and GPIO. It can be reasonably expected that it will be difficult to fit a more complex program involving EIS, cyclic voltammetry and chronoamperometry into 32kB. The Cortex M4F was therefore chosen due to its processing power, memory size and the fact that the BLE IC it comes with (nRF52832) is also very low power. It also has the most GPIOs which is important to interface with the components on the PCB, be it to communicate with specialised ICs via I2C or just to disable op-amps and put them into low-power mode.

The nRF52832 also has the advantage of having third party companies such as Sparkfun and Adafruit making breakout boards. These breakout boards come with preloaded serial bootloaders which make programming the on-board MCU much easier. The main advantage of these boards however are that the antenna comes built-in with these breakout boards. This goes back to the earlier point where it is undesirable to implement my own antenna, since it does not add any value in the context of this project but will consume large amounts of time due to the large likelihood that multiple revisions of the PCB are needed to get a correct, optimised and well-placed antenna.

The other advantage is that a low-dropout regulator (LDO) is included (but can be bypassed straight to supply voltage if the user desires). The acceptable supply voltage of the nRF52832 is rather low, ranging from 1.7 to 3.6V. Since it is desired that the system be run off batteries, there are two possible hardware configurations. One or more batteries with the maximum voltage below 3.6V when fully charged or use an LDO paired with batteries that have a minimum voltage when discharged to be above or equal to the LDO minimum input voltage. The most common rechargeable batteries (Lithium based such as Lithium Polymer (LiPo) and Nickel Metal Hydride (NiMH)) all have their nominal voltages dropping during their discharge cycle. This means that as the device is being used, dynamic range is being lost in all components of the circuit, such as op-amps, ADCs and DACs. This makes it less than optimal, especially considering that being powered by batteries often means that there is no negative supply rail, which already limits the dynamic range.

The other advantage is that it allows for direct powering from a commonly-found 5V USB charger, dropping the voltage from 5V to 3.3V. Otherwise, without the LDO, one will have to use a much more uncommon 3.3V output charger. However, the trade-off for using the LDO is that there is increased power consumption due

to losses in the LDO as the voltage is stepped down. This goes against the main design goal of keeping everything as low power as possible. In spite of this, the benefits of having a steady supply voltage outweigh the drawbacks and therefore the decision was made to run the batteries through the LDO. Both Sparkfun and Adafruit use the AP2112K LDO. From the datasheet of the AP2112K, it has a low quiescent current of  $50\mu\text{A}$  which is good from an efficiency viewpoint since there will be less power dissipated in the LDO. To make the LDO as efficient as possible, it will be desirable to have the battery voltage as close as possible to the onset of the regulation region. The regulation region is where the LDO works as advertised, with the correct output voltage. This directly impacts the decisions made in choosing a suitable battery for the device and will be discussed in detail in the battery subsection later.

It is also stated in the datasheet of the LDO that the maximum output supply current is limited to 600mA. This is the current budget that will be worked with in this project. In any case, 600mA is more than enough for the purposes of this PCB and will drain a battery too quickly. Additionally, the LDO is rated for 3.3V output. This influences the choice of the other components as their supply voltage range must include 3.3V unless there are no alternative components. This is to remove the need for any additional LDOs which will cause further losses or a boost converter which is noisy due to the high speed switching and is not suitable for low current measurement applications.

Considering all of the above, the decision was made to use the Sparkfun nRF52832 breakout board. The advantage it has over the Adafruit version is that Sparkfun gives access to 30 GPIO pins with 2 being used for reset and a status LED. Adafruit only give access to 19 GPIO, which may not be sufficient.

Finally, in terms of whether the Cortex M4F is sufficient, it is sufficient for both amperometry and cyclic voltammetry, both of which are not CPU intensive. The latter requires moderate amounts of memory to store the data which is present in the M4F. However, for EIS it is not sufficient. In fact, none of the processors are sufficient in the sense that the clock rate of the SPI is not fast enough. This will be elaborated upon in a later subsection when the EIS circuitry is discussed in detail. The reasons for why a separate, more powerful processor is not employed will also be detailed.

### 4.2.3 Potentiostat and current reading

With continuous monitoring, the sensors typically have to be driven all the time. The reason for this is that these sensors typically have a settling time before the current output is indicative of the metabolite level. While an EIS circuit would just be an extension of a standard potentiostat and current readout circuit, op-amps which are capable of amplifying up to a 1MHz signal are generally power hungry. To have these amplifiers on constantly means that the battery drain will be enormous. Consequently, this makes powering the device for at least 7 days on a single battery charge extremely difficult or even impossible when one considers that the battery has to be small and lightweight as well. This goes against the first design principle of this project, which is to keep the power draw as low as possible. The decision was therefore made to have 2 separate sets of circuitry. A low power one which can handle chronoamperometry and cyclic voltammetry.

The potentiostat was initially going to be based off the architecture seen in the research done by Alyssa et al. The team applied it in the context of fast-scan cyclic voltammetry to detect dopamine. The idea is to use a low precision ADC (about 10 bits precision) and gain extra resolution through analog BS. The reason for this is that a low resolution ADC will generally consume less power than a more precise 16 or 24-bit ADC, therefore helping to extend the battery life of the device. In fact, the integrated circuit (IC) consumed only about  $30\mu\text{W}$ [17]. It should be noted that this project will not be delving into designing custom ICs from the transistor level up (which is exactly what Alyssa et al. and her team did), therefore similarly low power consumption cannot be expected from this PCB.

The exact method involves using a 9-bit ADC and getting a rough measurement. This rough measurement will be stored in memory. A second measurement will be made, but this time with the first measurement being reproduced through a DAC which will be subtracted from the measurement in the analog domain. The result is then amplified and fed into the ADC to be stored as quantisation error. Both readings are then summed together as the final result of the measurement before being transmitted. The assumption here is that the dopamine levels do not vary significantly in between the two readings. To aid in understanding this, 2 diagrams from Alyssa et al. showing the exact circuit and the analog subtraction are shown in Figures 4.2 and 4.3. Note that in this implementation, this will not be used for BS but rather just to make measurements in general. Using this method, it is

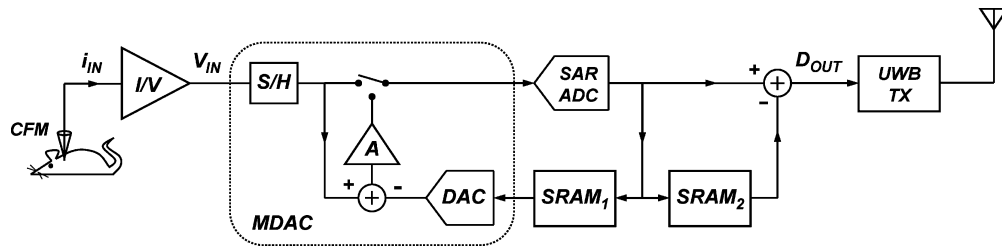


FIGURE 4.2: Removal of Quantisation Error with low resolution ADC[17]

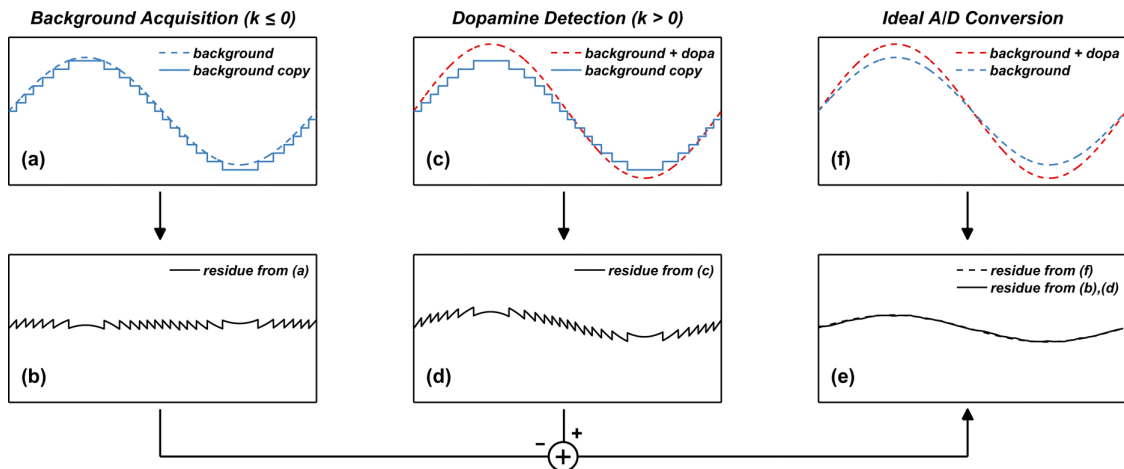


FIGURE 4.3: Circuit to perform analog subtraction[17]

shown that a 9-bit Nyquist ADC is able to obtain the same resolution as a 14-bit Nyquist ADC[17].

However, it is found that there are commercial Analog Front-End (AFE) ICs which have extremely low power consumption and are designed from the ground up to work with an electrochemical cell. There are currently 2 commercially available AFEs and both of them integrate the potentiostat with the transimpedance amplifier (TIA) necessary for current measurement. The 2 AFEs are the Texas Instruments LMP91000 and NJR NJU9101MLE-TE1 and are compared in Table 4.3. Note that SPS in the table means samples per second and therefore kSPS means kilosamples per second.

As we can see from the table, both ICs consume under  $10\mu\text{A}$  for the potentiostat. It is difficult to build a potentiostat from the ground up with discrete DACs and op-amps that have comparable levels of current consumption with the same low bias current and offset voltage.

For example, an amplifier which will outperform the above ICs is the new Texas Instruments LPV811 op-amp. It consumes just  $425\text{nA}$  of quiescent current, has offset voltage of  $300\mu\text{A}$  maximum and input bias current of  $100\text{fA}$ . However, it

Specifications/IC	LMP91000	NJU9101
Supply Voltage (V)	2.7-5.25	2.4-3.6
Supply Current (Active) ( $\mu\text{A}$ )	<10	4(potentiostat, TIA) + 150(ADC)
Supply Current (deep sleep) ( $\mu\text{A}$ )	0.6	0.5
Built-in TIA	Yes	Yes
Built-in ADC	No	Yes, 16-bit, 2kSPS
Potentiostat input bias current (pA)	90	10
Input Offset Voltage ( $\mu\text{V}$ )	$\pm 550$	$\pm 300$

TABLE 4.3: Table of Potentiostat AFEs

has a poor phase response and the manufacturer specifically states that it should not be used to drive capacitive loads greater than 50pF in unity-gain configuration due to the phase lag. Otherwise, there is a risk of oscillation. The manufacturer suggests using a resistor of 30k to 50k in series with the load, however, this leads to reduced headroom. On top of that, it can be expected that the capacitance of the sensors which will be paired with this PCB will have much greater capacitance. This is supported by Zhang's thesis in which the glucose sensor was found to have a capacitance on the order of  $\mu\text{F}$ [8], which is at least 5 orders of magnitude higher than the recommended load. This makes this op-amp unsuitable for this application.

The NJU9101 chip is preferred over the LMP91000 due to the lower power consumption of both the potentiostat and TIA and the fact that it comes with an integrated, extremely low power 16-bit ADC which is sufficient for this project as 16 bits give a resolution of 0.76nA at the maximum current required to be detected which is  $50\mu\text{A}$ . It also has a lower input bias current and input offset voltage, the former of which is very important in a three-lead electrochemical cell. The reason for this is that in an ideal cell, no current passes through the reference electrode (which is directly connected to the negative terminal of the driving op-amp) and therefore the cell potential (defined as Voltage of Working Electrode (WE) with respect to Voltage of Reference Electrode (RE)) is well defined. A consequence of this assumption is that the current passing through the cell only conducts through both the working and counter electrodes (CE). Therefore, a transimpedance amplifier at the WE will amplify the total cell current that passed through. Therefore a lower op-amp bias current is definitely preferred.

An equivalent ADC in terms of power consumption will be the Texas Instruments

ADS1114, which only samples at 860SPS but would still be fast enough for slow cyclic voltammetry. However, even with that, the NJU9101 potentiostat and TIA still consume less power than the LMP91002. If fast-scan cyclic voltammetry needs to be performed, then a new and fast ADC will be required in the case of both AFEs (NJU9101 allows access to the converted voltage after the transimpedance amplifier/before the ADC).

With that being said, it was logistically difficult to obtain the NJU9101 in the UK due to the fact that it is a newly released IC and UK suppliers such as Farnell do not have ready stock on hand. Therefore, the decision was made to go with LMP91000, which is still a good IC given the low power consumption of  $10\mu\text{A}$  when driving a cell. It has the further advantage of having a TIA which can be used independently of the standard potentiostat circuitry. This reduces the circuit complexity because the same low-power TIA can be used in cyclic voltammetry. Although it is not officially stated on the datasheet, it has been written on Texas Instrument's official forums by an employee of Texas Instrument that the bandwidth of the TIA is 10kHz[35]. This bandwidth is sufficient for slow-scan cyclic voltammetry, where we aim to do at most a few hundred millivolts per second in steps of approximately 5mV per step from the DAC.

#### 4.2.4 Analog-to-Digital Converter

Since the LMP91000 does not come with an ADC, an external ADC IC will have to be chosen. Based on the project specifications, for 3nA resolution at a maximum current of  $50\mu\text{A}$ , a minimum of 15 bits is required. To simplify the circuit, this same ADC will be used to process data for both cyclic voltammetry and chronoamperometry. In amperometry, the requirements are not so stringent. Apart from the aforementioned 3nA resolution, the ADC need only give a reading approximately every half an hour. The reason the readings are so sparse is because when in use to detect metabolites such as glucose, the levels of metabolite do not change rapidly in the body and take minutes. This is reflected in studies regarding metabolite levels in humans. For example, a study conducted into the effect of meal frequency on metabolic profiles including glucose and insulin show levels taken in intervals of half an hour to one hour[36].

On the other hand, cyclic voltammetry will require up to approximately 60 samples per second (300mV/s in 5mV steps). Therefore a sufficiently fast ADC (capable

Specification/ADC	ADS1114	MCP3421	ADS1148	AD7792
Vdd range (V)	2.0 - 5.5	2.7 -5.5	2.7 - 5.25	2.7 - 5.25
Current Consumption ( $\mu\text{A}$ )	150	145	212	400
Bits	16	18	16	16
Interface	I2C	I2C	SPI	SPI
Sampling rate (SPS)	860	3.5	2000	470
Input Voltage Range (V)	Up to $\pm\text{Vdd}$	$\pm 2.048\text{V}$	Up to $\pm\text{Vdd}$	Up to $\pm\text{Vdd}$
Integral Nonlinearity	1 LSB	35 ppm	1 LSB	15 ppm
Offset Error	3 LSB	$40\mu\text{V}$	1 LSB	$1\mu\text{V}$
CMRR (dB)	105	105	100	100
Output Noise ( $\mu\text{V}_{\text{rms}}$ )	62.5	1.5	62.5(p-p)	18.5

TABLE 4.4: Comparison of low-power ADCs

of minimum 60SPS) should be selected. A comparison of some of the available low-power 16 to 18 bit ADCs are shown in Table 4.4.

From the table, we can see that the MCP3421 has an insufficient input voltage range as well as an insufficient sampling rate. While it can go up to 240SPS, at that sampling rate it only has 12 bits of resolution, which is insufficient. The MCP3421 is immediately dropped from consideration.

Since the ADC is receiving the amplified signal from the TIA and does not interact directly with the electrochemical cell current, the output noise is not as critical as long as the effective bits remain at 15 and above. In terms of output noise, the three remaining are actually very similar, in that the noise does not cause any effective resolution loss and all three of them still have effective 16-bits. The nonlinearity and CMMR are all comparable, with their Vdd range all suitable for powering by batteries. The slowest sampling rate of the AD7792 is more than sufficient for the purpose of slow-scan cyclic voltammetry and therefore any of the three ADCs will be sufficient in this regard. With everything else being roughly comparable, the most important factor will then be power consumption. The AD7792 is the best performing of the three, but consumes more than twice the power of the ADS1114. The ADS1148 also consumes over 40% more than the ADS1114. Therefore, the decision was made to go with the ADS1114.

It should now be noted that none of these low-power ADCs will meet the requirements for EIS. EIS ideally requires a signal of up to 1MHz and by Nyquist sampling theorem, an ADC will need to be at least sampling at 2 million SPS. However, such ADCs are extremely power-hungry (details will be provided in the next subsection). Since EIS is performed only to calibrate the sensor, it can be expected

that this calibration will happen only once or twice a day. By comparison, amperometry happens much more often at the rate of every half hour. Therefore, in order to conserve battery life, the decision was made to have a separate, low-power ADC for the more frequent but much less technically demanding amperometry.



### 4.2.5 Impedance measurement

As stated, the requirements for impedance measurement that a range of  $100\Omega$  to  $2000\Omega$  be measured over as wide a frequency range as is possible (up to a maximum of 1MHz). The impedance measurement procedure for EIS is not so straightforward. Instead of applying an AC signal with a known amplitude and varying frequency with zero DC offset, here, the electrochemical cell has to be kept at a DC bias equal to the usual cell voltage (for example 0.53V for Zhang's glucose sensor) and apply a small amplitude AC signal on top of that. According to Bard and Faulkner, this AC signal is about 5mV peak-to-peak[6], which is also the amplitude used by Zhang[8]. The reasons for this are:

1. Having an infinitely steady response, allowing for high-precision measurements
2. Linearized/Simple models are a good fit for the current-potential characteristics with small signals
3. Ability to measure over a wide time/frequency range ( $10^{-6}$  to  $10^4$ s or  $10^{-4}$  to  $10^6$ Hz)

These benefits come about due to the fact that the electrochemical cell is near equilibrium from the DC biasing and allows for simplifications in both current-potential model as well as treating kinetics and diffusion[6]. All of these requirements make constructing the EIS part of the circuitry by far the most challenging part of designing the PCB.

Because the signal of interest is the AC signal, there is a chance that the AC current signal is small against a large DC background, especially with a much smaller AC voltage input. This means that the current signal is not utilising most of the range of the ADC and most of the range is used to detect the background DC current, which does not give any information in an EIS. If that is the case, it makes a potentiostat design particularly challenging due to the need for high-pass filtering to remove the DC.

In particular, the configuration used in the LMP91000 potentiostat IC, where the TIA is attached to the WE of the cell, will not be suitable. This is due to the additional function of the TIA of holding WE at virtual ground or  $V_{dd}/2$ .

To remove the DC current, either a simple first-order R-C filter at the negative terminal of the op-amp or a more complex second order filter such as a Butterworth filter can be used. However, these filters are AC-coupled to the input signal and therefore have no direct DC path. This removes the ability of the TIA to be able to pull the WE to a virtual ground. It is possible to get around this by attaching an inverting buffer with identical-valued resistors (such that no amplification occurs) to hold WE to virtual ground. This signal will then be passed into the high-pass filter before amplification.

Alternatively, a solution is to attached a resistor to the counter electrode and measure the current across that with an instrumentation amplifier. In this configuration, the WE is directly connected to ground or a fixed reference voltage (generally  $V_{dd}/2$ ). The inputs to the amplifier can be high-pass filtered and this will not affect the cell voltage. The issue with this solution is that having a large resistor for high gain can potentially saturate the control amplifier.

The other issue that arises with high-pass filtering is that we want to perform EIS down to very low frequencies. The LMP91000 can be used for DC measurements, but the AC measurement should be performed to as low a frequency as possible. For example, in Zhang's thesis, the EIS was performed starting from 10Hz[8]. For such low frequency high pass filters, large resistors and capacitors would have to be used. The problem with large-valued resistors is the relatively large amount of noise that will be introduced to the circuit. This is shown by the Johnson Noise Equation:

$$e_{\text{rms}} = \sqrt{4k_bTRf} \quad (4.1)$$

This is especially important for these electrochemical cells which produce low currents down to the range of nA.

However, Zhang's thesis shows that there are electrochemical cells, specifically the commercial CGMS sensor, which have AC impedances very much lower than DC impedance. This is inferred from the chronoamperometry readings which are on the level of nA with a cell voltage of 0.53V[8]. It can therefore be calculated that the DC impedance magnitude on the order of tens to hundreds of  $M\Omega$ . In contrast, the EIS measurements (which were conducted from 10Hz to 1MHz) give impedance magnitude values no greater than approximately 1.8k $\Omega$ . Even with

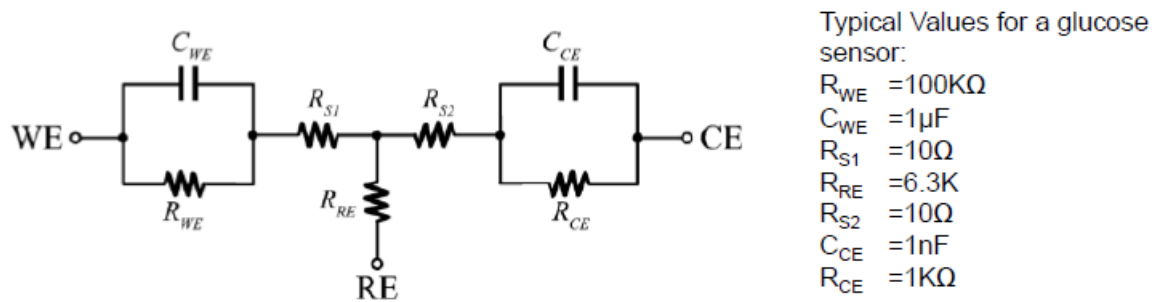


FIGURE 4.4: Equivalent model of a generic glucose cell[12]

only a 5mV peak to peak AC excitation, the current from the excitation is on the order of  $\mu$ A, which is three orders of magnitude higher than the DC current.

If this is the case, then the DC current can be ignored since it will not offset the AC signal significantly and most of the ADC range is used to measure the AC current. Because this is a big assumption to make, directly impacting the design of the device, further verification using both PSPICE simulation and testing on an actual sensor was carried out.

Randle's model is not used in the simulation because the Warburg Impedance value is frequency dependent, which is difficult to model in PSPICE. Instead, a generic equivalent model of an electrochemical cell is used instead, and it is shown in Figure 4.4. The schematic is shown in Figure 4.5 and the simulated data in Figure 4.6.

It should be noted that the circuit is a custom analog front end which will be discussed later on in its own subsection. For now, the results support Zhang's data. We can observe that the DC level of the output of the transimpedance amplifier (TIA in the schematic) has a DC level of 3mV with respect to 1.6V (split rail). However, from the data, we can see that the AC waveform is much larger, with a peak to peak amplitude of about 0.5V.

For the actual measurement, an identical sensor to the one used by Zhang was procured. To verify both DC and AC characteristics, both chronoamperometry and EIS were carried out on the sensor. Both measurements were carried out using the same bench instrument used by Zhang and with the sensor placed in similar test solutions. The test solutions are small amounts of 1M glucose solution mixed with 10ml of 100mM Phosphate Buffered Saline (PBS) solution to make solutions of 0mM (pure PBS solution), 2.5mM, 7.5mM and 10mM glucose. PBS

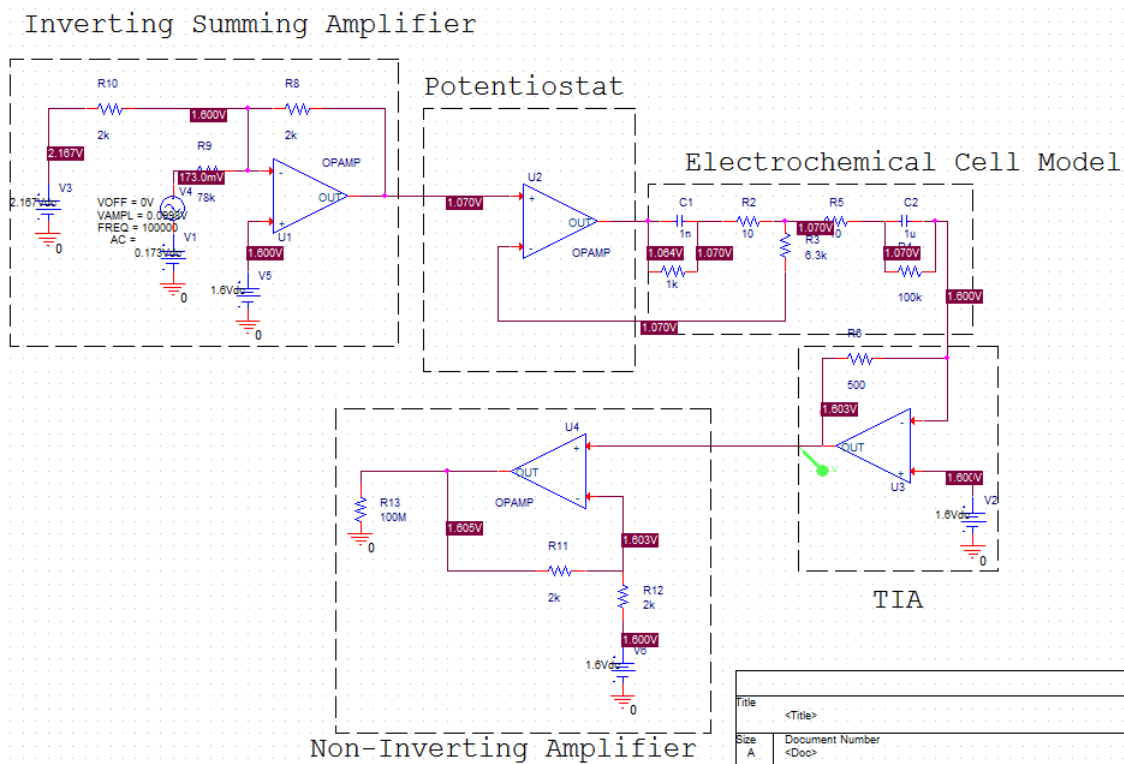


FIGURE 4.5: PSPICE Simulation

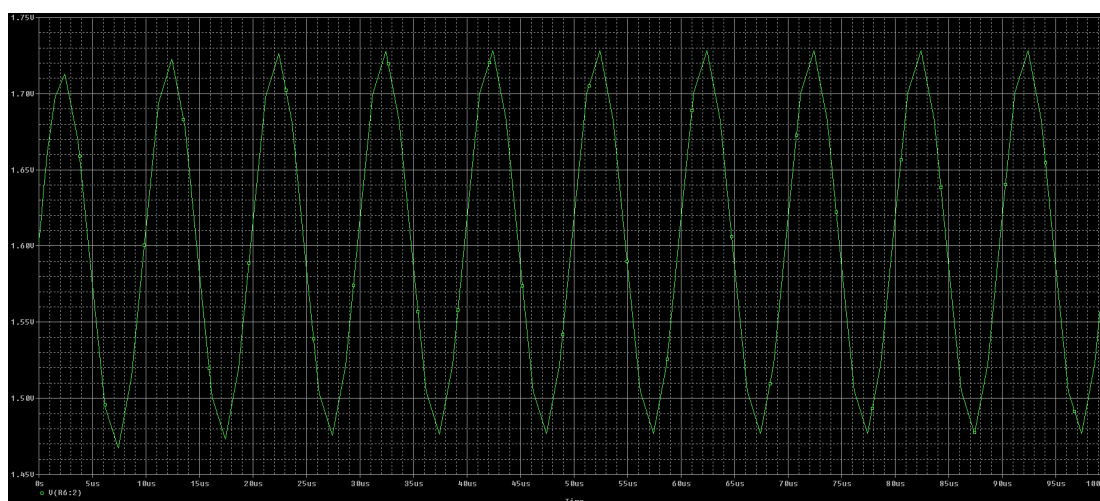


FIGURE 4.6: Simulated 100kHz waveform input

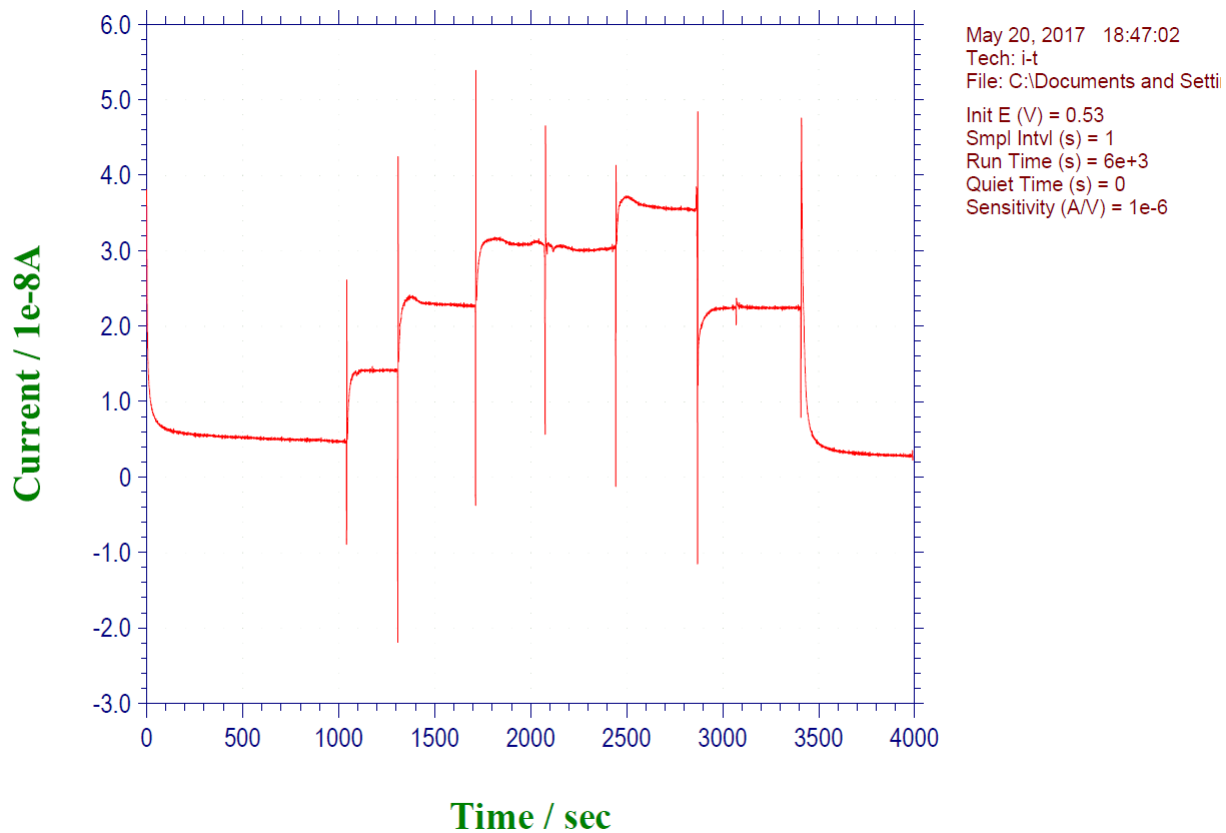


FIGURE 4.7: Chronoamperometry of CGMS Sensor

solution is used because it has similar ion concentrations (such as sodium and potassium), osmolality and pH levels to that found in the human body. This serves to more accurately simulate the sensor operation when it is actually being used on a human. The chronoamperometry results are shown in Figure 4.7 and the EIS results are in Figure 4.8.

It can therefore be seen that even with a maximum measured 35nA current readout at DC, it is shown that this is much smaller than the minimum AC current which is  $5\text{mV}/1\text{k}\Omega = 5\mu\text{A}$ . Therefore, Zhang's findings are verified. In this case, the standard potentiostat and TIA at the WE configuration will suffice.

For impedance measurement, the only AFEs available to the best of my knowledge are the Analog Devices AD5933 and AS5934, which are identical except that the AD5933 has a 1MSPS ADC and an internal temperature sensor whereas the AD5934 has a slower 250kSPS ADC with no temperature sensor. The specifications for the AD5933 are shown in Table 4.5 and the simplified block diagram in Figure 4.9:

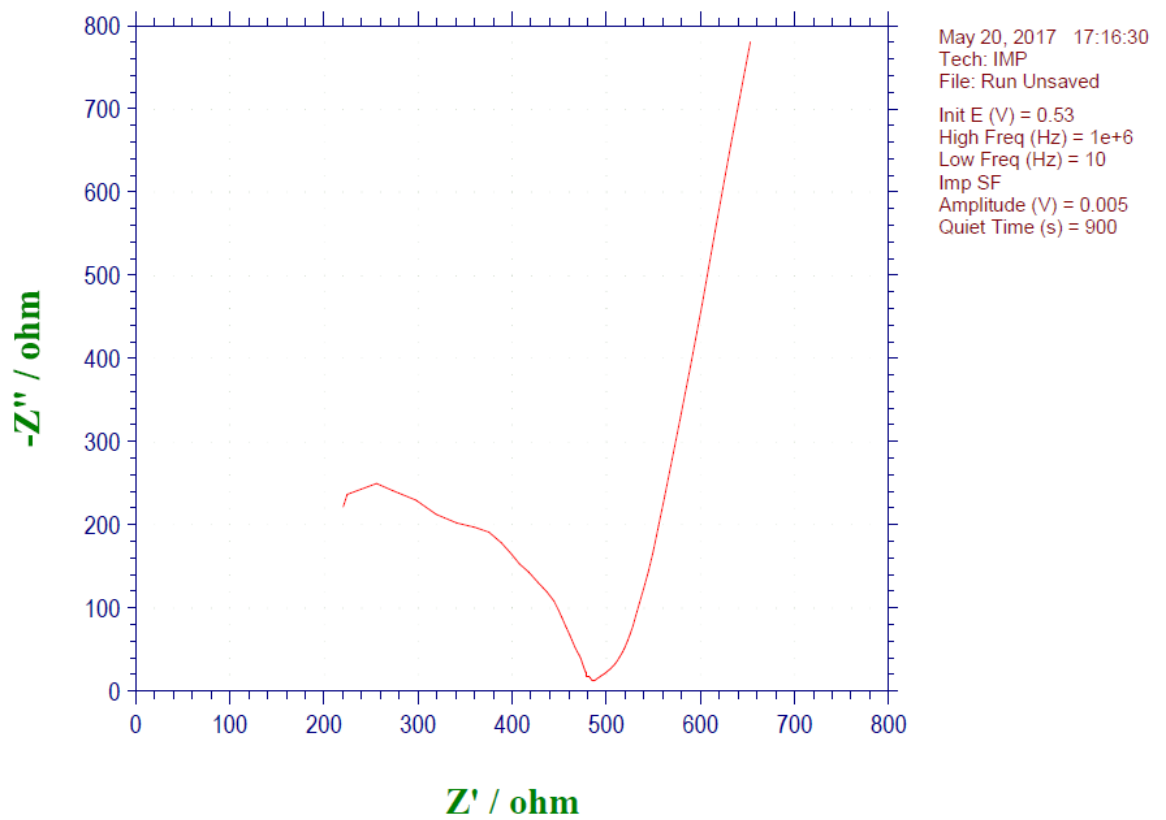


FIGURE 4.8: EIS of CGMS Sensor

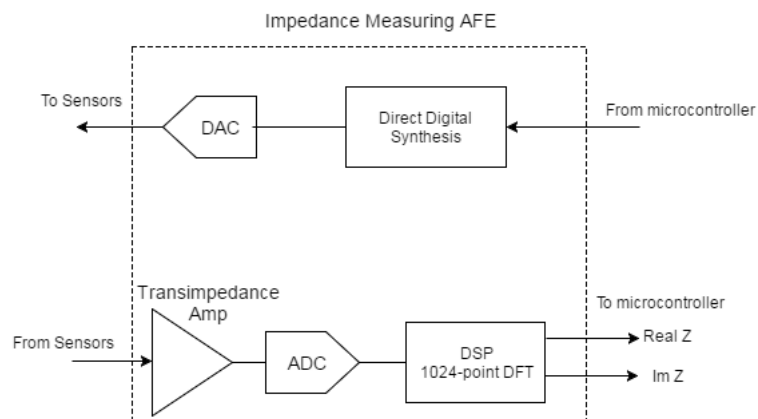


FIGURE 4.9: Analog Devices AD5933 Simplified Block Diagram

Specifications/IC	AD5933
Supply Voltage (V)	2.7-5.5
Supply Current (Active) (mA)	10-17
Supply Current (deep sleep) ( $\mu$ A)	0.7
Impedance Range ( $\Omega$ )	1k-10M
Output Frequency Range (Hz)	1k-100k
Output Frequency Resolution (Hz)	0.1
ADC Resolution (Bits)	12
ADC Sampling Rate (MSPS)	1
On-board DSP Engine	1024-point DFT

TABLE 4.5: Table of AD5933 Specifications

Note that for the impedance and frequency range, Texas Instruments officially state in their datasheet that the AD5933 will work down to  $100\Omega$  range with additional circuitry and the lower limit of the frequency range can be lowered by scaling down the input clock. In addition, Chabowski et al show that it can be made to work down to  $10\Omega$  and 1Hz[37]. In practice, to be able to acquire such low frequency readings require a slowing down of both the input clock to the AD5933 as well as slowing down the I2C clock from the master device.

As can be seen from the table, the AD5933 does not fully fit the specifications of this project, even after the modifications. It is not guaranteed to go down to DC (and in fact is unlikely to go down to exactly DC, but 1Hz is close to DC and proven possible) and does not go up to 1MHz. The impedance range however is good and the fact that it comes with an on-board DSP which makes application development on mobile platforms such as mobile phones and tablets more likely. It does come at the cost of higher power consumption however, in the region of tens of mW when in operation, which is undesirable.

One method to extend the upper limit of the frequency range to 1MHz would be using analog mixers such as the Linear Technology LT5560 and a TIA. This of course also requires a way of generating a variable frequency clock signal such that the input oscillator frequency into the mixer can be varied. The idea is, in the block diagram, the mixers will be placed between the DAC and the sensor to upconvert the frequency such that they are in the range 100kHz to 1MHz as well as between the external TIA and ADC on AD5933 to downconvert the voltage signal back. However, this will prove to be tricky given that the AD5933 does not allow access to the ADC input. It is also unclear how a mixer will alter the

Specs/Waveform Gen	MAX038	AD9833	AD5932	AD9106
Active Current (mA)	35 + 45 + 1	4.5	6.2	Up to 82.5
Vdd range (V)	4.75-5.25	2.3 - 5.5	2.3 - 5.5	1.7 - 3.6
Freq Range (Hz)	0.1 to 20M	0 to 12.5M	0 to 25M	Up to 180M
Output Resolution (Bits)	N/A	10	10	12
Output Voltage (V <sub>p-p</sub> )	2	38m to 650m	0.58 with 56m DC	N/A
Output Current (mA)	NIL	NIL	NIL	2 to 8
Sleep Current ( $\mu$ A)	N/A	500	20	<1400

TABLE 4.6: Table of Waveform Generators

current and voltage given that commercial mixer ICs always rate them in terms of power gain in dBm.

Alternatively, with no dedicated AFE, the next best option is to reuse the potentiostat AFE, which shares many of the same components required sans the DSP and direct digital synthesis (DDS) to generate the sine wave output to the sensor via the DAC. Direct digital synthesis can be achieved with a circular buffer or a queue in the microcontroller, and as previously mentioned, DSP can be brought to the receiving laptop or mobile phone. Again, this will require mixers as the chosen ADC only does up to 860kSPS but it is difficult to find mixers that are rated for such a low frequency.

The final method will be to use discrete components to measure the current with the necessary high speed DDS + DAC, high speed ADC and TIA. First, possible waveform generators were looked into as shown in Table 4.6. The reason dedicated ICs are wanted is because for impedance measurement, it is desirable to have a clean, pure sine wave which dedicated waveform generator ICs are designed for. It also removes the burden on the MCU to consistently update the DAC to generate a sine wave (this will be done by the DDS onboard the waveform IC) whilst reading back results from 2 high speed ADCs.

The MAX038 is not so desirable because it uses external resistors and capacitors to tune it to a single frequency. This makes it unsuitable for the purposes of frequency sweeps which is what happens in EIS. The other three can be programmed by a MCU and output the desired frequency. Amongst the three remaining, any one of them will meet our criteria since it is only required to go up to 1MHz. Therefore, the decision was made based on power. The AD9106 is overly powerful for our purposes and consumes a lot of power in both active and sleep modes. Hence the choice is narrowed down to the AD5933 and AD9833. Since EIS only happens



Specs/ADC	MAX11329	AD7621	LTC2313-12	LTC1403
Active Power (mW)	15.2	70	14	14
Sleep Power ( $\mu$ A)	2	240	7.6	10
Vdd range (V)	2.35 - 3.6	2.35 - 2.65	2.35 - 3.6	2.7 - 3.6
Sampling Freq (MSPS)	3	3	2.5	2.8
Resolution (Bits)	12	16	12	14
SPI SCLK (MHz)	48.1	80	90	50.4

TABLE 4.7: Table of high speed ADCs

infrequently, the IC will be in sleep mode for a majority of the time. Therefore, the AD5932 was chosen for having much lower sleep current at the cost of higher active current compared to the AD9833.

High speed ADCs were then looked into. As a point of reference, the bench instrument that was used by Zhang to perform EIS has a 16 bit resolution. The table of suitable ADCs are shown in Table 4.7.

This is where the problem mentioned before in the MCU section arises. All high speed ADCs require high speed SPI clock rates (minimum of 48MHz) from the master device to be able to perform at their advertised sampling frequency. On top of that, a general MCU needs to run at least twice as fast in order to be able to capture data from 2 high-speed ADCs. Such high speed SPI are not supported by any of the BLE chipsets that have been presented.

Therefore, new MCUs were looked into. It was found that MCUs which have SPI buses that support such high speeds are all power hungry, high clock rate processors. These include high performance microcontrollers, high speed DSPs, complex programmable logic devices (CPLD) and FPGAs. As mentioned before, in general FPGAs are not suitable for portable use. There are a few which have been advertised as low power, such as the Lattice Semiconductor iCE40 UltraLite™. However, they come with low internal oscillator speeds. The aforementioned iCE40 comes with a 48MHz clock. This clock is then used to synchronise SPI operations. This means that SCLK is not going to be faster than 48MHz at best, which just falls short of operating a MAX11329 ADC. Furthermore, they come with limited logic cells and storage. The iCE40 has 4kB of fast memory, which is not enough to store data for a 1024 point DFT, even at the minimum resolution of 12 bits. Additionally, FPGAs need to be reprogrammed every time it is powered down, typically with a computer environment and the relevant program from the manufacturer. This is undesirable for a portable device where the batteries may be

run to empty by the user. CLPDs do not have this issue, and even low power CLPDs such as the MAX V family of CLPD from Altera can run at over 200MHz. However, again there is simply not enough storage for the user, with just 8kB of flash memory.

DSPs which are fast enough include the Texas Instruments TMS320C5517, which will generate an SPI SCLK of 50MHz at an internal clock rate of 200MHz. However, at 200MHz, the DSP alone is consuming almost 250mW of power, which is too much for our application and it can be expected that the EIS will take a relatively long time at low frequencies so that at least a full period of the waveform is captured in 1024 samples. This is to ensure the best accuracy since DFT involves treating the sample data as 1 period of a periodic sequence. With an AC sine wave, the signal is actually periodic and the full information is contained within 1 cycle of the sine wave. Therefore a minimum of 1 period must be captured for full accuracy.

Finally, high performance microcontrollers which just fall short of 48.1MHz SPI speeds include the ARM A series. Example MCUs include Texas Instruments AM437x Sitara™ Processors which use an ARM A9 clocked up to 1GHz. These processors have much more power and memory than we require. However, the A9 series processors have power consumptions of around 500mW, which again is too much for this application.

Therefore, it was decided to stick to using just the Cortex M4F that we already have and try and get as much performance out of it as possible. Using a waveform IC, it is still required to capture the AC voltage output of the IC synchronously with the current from the sensor as the AD5932 does not give direct access to the digital representation of the sine wave from the DDS. Given that the SPI on the nRF52832 gives a maximum clock rate of 8MHz and that 2 ADCs need to be read simultaneously, at maximum it is possible to obtain just over 330kHz sampling with 12 bit ADCs. This allows for an AC signal of no more than 165kHz according to the Nyquist theorem.

If that is the case, that is not much better than the AD5933 impedance analyser IC. The IC is rated by the manufacturer to be accurate up to 100kHz, which is not much less than 165kHz. Moreover, other researchers have successfully used the AD5933 at higher rates. This is due to the fact that the AD5933 has a 1MSPS ADC built-in but the manufacturer only guarantees results up to 100kHz.

For example, Bogónez-Franco et al. have used it up to 200kHz for bioimpedance measurements with a maximum error of 2.5% in impedance magnitude and 4.5% in phase[38]. The impedance range used was 10 $\Omega$  to 1 k $\Omega$ , which partially covers this project's impedance range of interest (100 $\Omega$  to 2k $\Omega$ ). Separate research carried out by Ferreira et al. have successfully used the AD5933 up to 450kHz for bioimpedance measurements with textile electrodes[39]. The team managed to get a maximum error of 0.7% in resistance and 17% with reactance. The impedance range measured is not explicitly state, although based on the graphs from the conference paper, the resistance is between 300 $\Omega$  to over 600 $\Omega$  and the reactance is between 0 $\Omega$  and just over 100 $\Omega$ .

Therefore, the AD5933 is chosen due to potentially higher bandwidth than using a waveform IC and ADC. In addition, it gives the benefit of removing the burden of synchronous detection from the MCU, which may prove to be very difficult at high frequencies.

#### 4.2.6 Programmable Clock

While the AD5933 comes with an on-board oscillator to act as a clock, Analog Devices recommend on their design notes that for measuring signals below 5kHz, it is best to provide an external clock with a lower clock frequency. The reason for this is due to the resolution of the DFT. With a 1MHz sampling and 1024 data points, the DFT has a resolution of approximately 1MHz/1024 = 1kHz. Below 1kHz, the accuracy of the impedance measurement greatly decreases due to spectral leakage. The recommended clock frequencies from the design notes are shown below in Figure 4.10.

In general and more optimally, the frequency being measured should be no less than the clock frequency divided by 1600. The maximum that it can go to is 16000 times less than the clock frequency before Analog Devices claim that the error becomes too great.

Since EIS is performed down to a minimum of 10<sup>-4</sup>Hz, a minimum of 1kHz is not good enough for our purpose. The goal is to replicate the range that Zhang used in his research, which extends down to 10Hz, if not lower.

Therefore, an external clock needs to be provided. However, it is not optimal to simply add a slow oscillator. The reason for this is that the external clock

AD5933 Lower Frequency <sup>1</sup>	Clock Frequency Applied to MCLK Pin <sup>2</sup>
100 kHz to 5 kHz	16 MHz
5 kHz to 1 kHz	4 MHz
5 kHz to 300 Hz	2 MHz
300 Hz to 200 Hz	1 MHz
200 Hz to 100 Hz	250 kHz
100 Hz to 30 Hz	100 kHz
30 Hz to 20 Hz	50 kHz
20 Hz to 10 Hz	25 kHz

<sup>1</sup> Lower frequency sweep limit established by applying the divided clock signal to the MCLK pin of the AD5933 and by calibrating and remeasuring a nominal impedance  $Z_{\text{CALIBRATION}}$ , for example, a 200 k $\Omega$  resistor over a 500 Hz linear sweep from the programmed start frequency (I-V gain resistor setting =  $Z_{\text{CALIBRATION}}$ , for example, 200 k $\Omega$ , PGA = X1,  $\Delta$ Frequency = 5 Hz, and number of points = 100). The lower frequency limit is established as the frequency at which the DFT and, therefore, the impedance vs. the frequency results begin to degrade and deviate from the expected value of the measured impedance  $Z_{\text{CALIBRATION}}$ , for example, 200 k $\Omega$ .

<sup>2</sup> TTL clock levels applied to MCLK pin,  $V_{\text{IH}} = 2$  V, and  $V_{\text{IL}} = 0.8$  V.

FIGURE 4.10: Recommended clock frequencies for AD5933[40]

Specs/Clock IC	DS1077LZ-40+	LTC6904	DS1085L
Vdd Range (V)	2.7 - 3.6	2.7 - 5.5	3.0 - 3.6
Active Current (mA)	15	15	15
Sleep Current ( $\mu$ A)	5	2200	1500
Frequency Range (kHz)	4.87 - 40000	1 - 68000	4.1 - 66000
Output Freq Tolerance	$\pm 0.5\%$	1.6%	$\pm 0.75\%$
Jitter	50psec	1%	NIL

TABLE 4.8: Programmable Clock ICs

also becomes the system clock for the AD5933 IC. Consequently, the ADC is also clocked by this system clock and will operate at: (system clock divided by 16) samples per second (originally, internal clock is 16MHz which is why the ADC is normally at 1MSPS). This directly impacts the maximum frequency that can be detected. A very slow oscillator also causes impedance measurements to be slower since the entire IC is now being clocked at a slow rate.

Hence, multiple oscillators with different frequencies need to be provided. This solution however, is not optimal due to the fact that attaching so many different oscillators can couple more noise onto the sensitive analog circuit with the sensor and also increases the circuit complexity. A better solution is to use a programmable clock IC. There are not too many programmable clocks which extend down to a very low frequency, which is what is required for this. Table 4.8 shows some of the available ICs.

It can be seen from the table that the DS1077LZ-40+ is the optimal programmable clock to use. It has low jitter, the lowest frequency tolerance and lowest sleep current. The frequency range is also suitable for this application, where Analog Devices recommend external clock frequencies from 25kHz to 4MHz. Therefore, the DS1077LZ-40+ was chosen.

#### 4.2.7 Custom AFE for impedance measurement

As explained previously, due to way EIS is performed, AD5933 output excitation sine wave needs to be scaled down and DC biased correctly. On top of that, the AD5933 is designed for two-terminal devices. The sensors that this PCB is designed for will have three terminals, one each for WE, CE and RE. Therefore a custom analog front end (AFE) is added to the AD5933 for the EIS. The diagram is exactly the same one as before from Figure 4.5. The only difference is that a 100M $\Omega$  resistor is used as a dummy load and the DAC, AD5933 and a voltage reference (1.6V. Will be explained later in this section) are replaced by DC and AC sources with the corresponding values. The electrochemical cell sensor is also replaced by the equivalent model from before.

The first part of the AFE starting from the Vout of the AD5933 impedance meter comprises of an inverting summing amplifier to add the AC sine wave to a DC bias which will be generated from a DAC. The selection of the DAC will be discussed in the next subsection.

The output of the AD5933 has a few selectable levels of peak to peak voltage and DC offset. From the datasheet, the smallest voltages are 0.198Vp-p with DC bias of 0.173V. Therefore, the resistor value for this branch of the summing amplifier is set at 78.7k $\Omega$  (deliberately chosen to be a value easily found in Surface Mount Device (SMD) resistors), with the feedback resistor set to be 2k $\Omega$ . This attenuates the sine wave to be 5.03mVp-p with a DC bias of 4.39mV.

The output of the summing amplifier is then fed into an op-amp which acts as the control amplifier for the potentiostat. An alternative configuration for the control amplifier (shown in Figure 4.11) was to use a non-inverting buffer on the RE so that a positive cell voltage can be established with a positive Vin, which is what is required here. However, this configuration has a flaw in that high frequency signals need to be sent through the electrochemical cell. This configuration is typically

used in chronoamperometry, where the signal changes slowly. With high frequency signals, the response of the control amplifier and buffer are less predictable. This could potentially lead to instability due to the extra buffer in the feedback loop of the control amplifier. Hence, a single op-amp solution for the control amplifier was chosen.

With a single op-amp, it is not possible to generate a positive cell voltage if the WE is connected to virtual ground via the TIA. Therefore, the supply rail needs to be split and  $V_{dd}/2$  used in place of ground for the entire AFE.

To do this, there were several options:

1. Use a simple resistor divider
2. Use a resistor divider followed by an op-amp buffer
3. Use a voltage reference IC

The first option requires a trade-off between noise and current drawn. With higher value resistors, the current drawn becomes less, but the noise will be greater. Furthermore, the resistor divider should have a low impedance compared to the input impedance of the circuit that the divider is connected to. Otherwise, the resistor divider no longer works as expected due to the current draw from the circuit being comparable to that in the divider.

The second option removes the restriction that the resistor divider needs to be relatively low impedance and better ensures the stability of the divider. The divider will now output the expected voltage over a much larger range of circuit input impedances. The trade-off comes in the form of increased power consumption due to the extra op-amp buffer.

The third option is the most attractive, especially when we consider that there are voltage references with extremely low current consumption and can source up to a few mA. Since this split rail is only connected to op-amp inputs, the current drawn will not add up to a few mA and this solution is the one that was chosen.

The IC that was picked is the MAX6018. It provides a 1.6V reference (which is close to  $V_{dd}/2$  of 1.65V), has an accuracy of 0.2% and a low supply current of less than  $5\mu\text{A}$ . In comparison, to get a resistor divider with such a low power consumption, a total impedance of  $660\text{k}\Omega$  needs to be used, which is not suitable

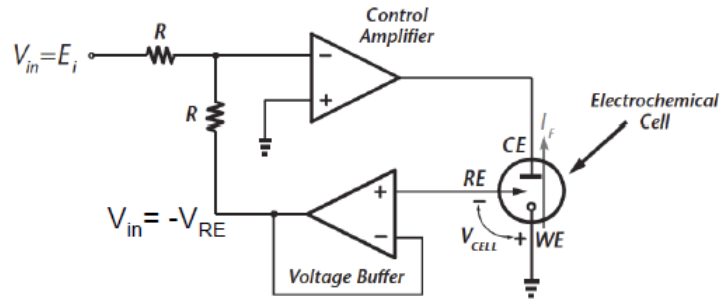


FIGURE 4.11: Alternative Potentiostat Configuration[12]

Specs/Op-Amp	LTC6268-10	ADA4895-1	THS4302	MAX4212
Active Current (mA)	16.5	6	46	120
Sleep Current ( $\mu$ A)	1200	10	1200	400
Vdd range (V)	3.1 - 5.25	3 - 10	3 - 5	3.15 - 11
0.1dB Bandwidth (MHz)	10	8.9	NIL	50
3dB Bandwidth (MHz)	200	236	875	300
Unity Gain Bandwidth (MHz)	4000	9000	12000	NIL
Voltage Noise ( $\text{nV}/\sqrt{\text{Hz}}$ )	4	1	2.8	10
Current Noise ( $\text{pA}/\sqrt{\text{Hz}}$ )	0.007	1.6	NIL	1.3
Input Bias Current (nA)	0.000003	16000	13000	20000

TABLE 4.9: Comparison of Op-Amps

due to the high resistance without buffering.  $660\text{k}\Omega$  resistance will also introduce noise. As a general rule of thumb, resistor values close to  $1\text{M}\Omega$  and above are considered to introduce too much noise into this AFE.

The next step is to select the op-amps that will be used in this AFE. A selection of high bandwidth op-amps which will work with a supply voltage of  $3.3\text{V}$  are shown in Table 4.9.

The control amplifier and TIA are chosen to be the LTC6268-10. The reason for this is that it has an extremely low input bias current of  $3\text{fA}$ . In comparison, none of the other op-amps even come close to matching this. This is important since one of the inputs will be directly connected to RE. It is desirable that extremely low current flows in RE such that the assumption that all current flows only through CE and WE holds true. The LTC6268-10 satisfies this condition even for very low cell currents of nAs, as the bias current is at least 6 orders of magnitude lower. It also has outstanding voltage and current noise levels. In fact, this op-amp was designed to be used as a TIA, and the same reasons apply as to why it is chosen as a TIA. With low bias current, most of the cell current will enter the feedback

$$f_{GBW} > \frac{C_{IN} + C_F}{2\pi R_F C_F^2}$$

FIGURE 4.12: Equation relating bandwidth with gain for TIA

resistor instead of being used to drive the op-amp bias current. This ensures a very accurate voltage output from the TIA.

However, with respect to the TIA, the bandwidth of the op-amp is not enough for a sufficiently large gain to be applied across it. The gain of a TIA is simply the value of the feedback resistor. The equation relating gain and the bandwidth of the amplifier is shown in Figure 4.12.  $f_{gbw}$  on the left hand side is the unity gain bandwidth of the amplifier,  $C_{in}$  is the input capacitance seen by the op-amp,  $C_f$  is the feedback capacitance which is used to help stabilise the TIA and finally,  $R_f$  is the feedback resistance.

The input capacitance of the electrochemical cell can be inferred from Zhang's thesis. It is found that the sensor that he was testing had a high capacitance value on the order of  $\mu A$ . This high value is contributed by the Warburg capacitance and will decrease with increasing frequency. The frequency independent capacitance is noted to be on the level of nAs. However, since it is desired to go to a low frequency, this is the maximum capacitance that can be seen by the op-amp. It is calculated that for a bandwidth of approximately 10MHz and this high input capacitance, the maximum safe resistor value is 10k $\Omega$  with a feedback capacitor of 10pF.

Since the PCB is designed to work with EIS impedance values of minimum 100 $\Omega$ , the maximum current that is expected is 50 $\mu A$ p-p with an excitation of 5mVp-p. After amplification by the TIA, the current is amplified to 500mA. This is not the full dynamic range that is possible. With the TIA output centered around 1.6V and a supply of 3.3V, it is possible to amplify the signal further. In this case, a second non-inverting amplifier is used to amplify the signal further by 6 times, to being the signal to 3Vp-p. This allows for some headroom since op-amps will not reach the full range given by the supply voltage.

The op-amp chosen for the summing amplifier and non-inverting amplifier is different to the one used for the TIA and control amplifier. The reason for this is that the LTC6268-10 is quite power hungry when active, with a current draw of 16.5mA. It is preferred to have a lower power op-amp which has higher bias current and noise values. This is because the current signal has already been amplified



by 10000 and the higher noise values are much less significant compared to the amplified signal. Therefore, the trade-off was made in order to have better battery life. The op-amp chosen is the ADA4895-1. It has the lowest active power consumption of 6mA and a good sleep current draw of  $10\mu\text{A}$ . On top of that, while the current noise is higher, the value is still very small, on the order of pAs. In fact, the ADA4895-1 outperforms the previous LTC6268-10 in terms of voltage noise.

## 4.2.8 DAC and Analog Switch

As mentioned earlier, the DAC is required to perform the offset required to properly bias the electrochemical cell. The DAC will also be used for cyclic voltammetry as the LMP91000 potentiostat that was chosen does not have fine control over  $V_{\text{cell}}$ . It allows for 0%, 1% and subsequently 2 to 20% in steps of 2% of either the supply voltage or a reference voltage to be applied across the cell. This is insufficient for cyclic voltammetry, where it has been established that the minimum resolution is 5mV. The LMP91000 allows the TIA to be used with the control amplifier for the potentiostat turned off. In this case, cyclic voltammetry will be carried out by using the potentiostat from the custom AFE and the TIA circuitry embedded in the LMP91000. In this way, the power draw can be reduced since only 2 power hungry op-amps from the custom AFE need to be turned on instead of the full AFE being powered up. With a supply of 3.3V, cyclic voltammetry will require 660 steps, which can be fulfilled by a 10 bit DAC. For biasing the cell during EIS, it is desirable to have resolution down to 1mV, in which case there are 3300 steps and a 12 bit DAC will suffice.

A comparison of suitable DACs is shown in Table [4.10](#).

For the DAC, one of the most important criteria is the active current draw. The reason for this is that as stated in a previous paragraph, the LMP91000 does not have fine control over the  $V_{\text{cell}}$  that can be set if only the supply voltage is used. If a different  $V_{\text{cell}}$  is required, then an external reference which can be divided into the appropriate cell voltage needs to be provided. Therefore, the DAC needs to also act as a reference voltage for the LMP91000 potentiostat. If that is the case, the DAC will be powered on all the time together with the LMP91000. Based on this requirement, the DAC8411 will be best suited. Although it has the highest sleep current, the sleep currents are all in the range of nAs and therefore even

Specs/DAC	DAC8411	MCP4725	AD5621
Active Current ( $\mu\text{A}$ )	95	210	100
Sleep Current (nA)	400	60	200
Vdd range (V)	1.8 - 5.5	2.7 - 5.5	2.7 - 5.5
Resolution (Bits)	16	12	12
Interface	SPI	I2C	SPI
INL Error (LSB)	$\pm 4$	$\pm 2$	$\pm 1$
DNL Error (LSB)	$\pm 0.5$	$\pm 0.2$	$\pm 0.5$
Gain Error (% of FSR)	0.05	-0.1	0.0004
Offset Error (mV)	$\pm 0.05$	0.02% of FSR	$\pm 0.063$

TABLE 4.10: Table of DAC

with 400nA, the battery life is not significantly affected if the DAC is not used to provide a reference for the potentiostat IC.

The DAC8411 also has the advantage of having more bits than is required. Since the integral and differential nonlinearity errors are quoted in terms of LSB, the error is much less than the 1mV precision that is required. This ensures that the cell voltage can be set accurately and meet the specifications.

Therefore, the decision was made to use the DAC8411.

Finally, in order to be able to switch between connecting the LMP91000 potentiostat or the custom AFE to the sensor, low impedance analog switches are used. Under consultation from my supervisor Dr Sara Ghoreishizadeh, the sensors can be thought of as low pass filters, which is why steps of 5mVs are acceptable for cyclic voltammetry. In this case, it means that the switching, as long as it takes milliseconds, can be assumed to not adversely affect the connected sensor. Therefore a low resistance analog switch DG2731 made by Vishay Siliconix was used. It has a very low impedance of just  $0.4\Omega$  and a switching time of 50ns. This fully meets the requirements for switching time. On top of that, it consumes at most  $1\mu\text{A}$ , which is good for battery life.

## 4.2.9 Batteries

The batteries would ideally be rechargeable. This makes it more convenient for the user as the user does not need to keep buying batteries. Based on power estimates drawn from datasheets, the worst case power consumption of the EIS is 108mA and amperometry will take approximately 2mA, with the current draw going up

Specs/Battery	VARTA 55750403015	VARTA 55625603059	VARTA 55960201012
Technology)	NiMH	NiMH	NiMH
Voltage (V)	3.6	3.6	1.2
Capacity (mAH)	500	250	580
Weight (g)	46	33	14.5
W x L x H (cm)	3.65 x 7.35 x 0.8	2.68 x 2 x 2.6	3.41 x 2.41 x 0.66
Type	Battery pack with XHP-3 connector	Button Cell	Button Cell
Charge Cycles	NIL	1000	1000

TABLE 4.11: First table of batteries

Specs/Battery	Ansmann 5035222	ENERGIZER NH15-2000	103456A-1S-3M
Technology)	NiMH	NiMH	LiPo
Voltage (V)	1.2	1.2	3.7
Capacity (mAH)	1100	2000	2050
Weight (g)	13	30	45
W x L x H (cm)	1.05 x 4.45	1.45 x 5.05	56 x 36.5 x 10.7
Type	AAA	AA	Battery Pack
Charge Cycles	500	1000	NIL

TABLE 4.12: Second table of batteries

to 6mA when the MCU wakes up to attend to BLE connections. Assuming that EIS needs to be carried out twice a day, with each session lasting 15 minutes (a conservatively long time) and the rest of the time is spent in amperometry, a 800mAH battery should help meet the target of 7 days. Note that cyclic voltammetry is not accounted for here as it is not normally done under normal usage. Amperometry will give the metabolite reading and EIS will calibrate the sensor. Cyclic Voltammetry will only be done on demand when a command is issued from the connected PC or mobile phone.

A table of rechargeable batteries is shown in Tables [4.11](#) and [4.12](#).

It can be seen from the first table that the button cells do not meet the required capacity for the PCB. This narrows the choice down to NiMH AA, AAA and LiPo battery packs. NiMH batteries have an advantage of having operating voltages which are stable at 1.2V through most of its discharge cycle (seen in Figure [4.13](#)). This means that to power the PCB, 3 cells in series to make 3.6V is sufficient. At the end of the discharge cycle, the cell voltage drops to around 1.0 to 1.1V, which makes 3.0 to 3.3V. Based on the datasheet of the LDO, at 3.0V the LDO will

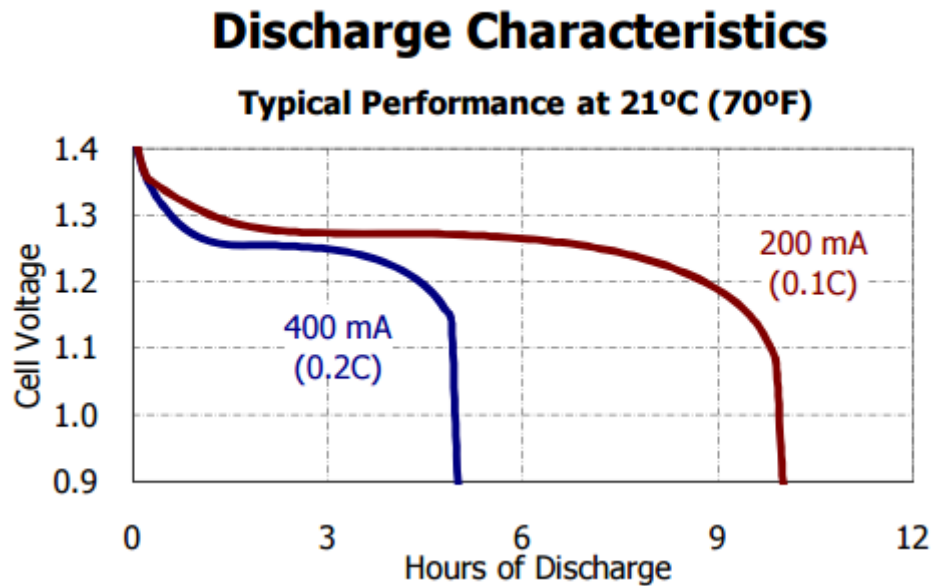


FIGURE 4.13: NiMH Discharge Graph

output 3.0V typically and 3.3V will also output approximately 3.3V. 3.0V is still within the working range of most of the components that have been selected for the PCB (except for the LTC6268-10). However, at that battery level, the MCU should detect it and shutdown the PCB to prevent overdischarge of the batteries anyway. In fact, Figure 4.13 shows the actual discharge curve of the Energizer AA cell in Table 4.12, and it can be seen that the cut-off is approximately 1.1V, beyond which the voltage decreases rapidly, indicating that the cell is fully discharged.

As stated early on in this section when the MCU was discussed, the closer the voltage is to the onset of the regulation region, which according to the datasheet is approximately 3.5V, the lower the losses through the LDO. The voltage of 3.6V fits this perfectly.

In contrast, LiPo batteries have a nominal voltage of 3.7V, but the voltage varies widely from 4.3V at full charge down to approximately 3.0V when fully discharged (as seen in Figure 4.14 which depicts a generic LiPo cell). In fact, for the LiPo battery shown in Table 4.12, it is fully discharged at 2.75V, which is dangerously close to the lower limit for some of the ICs such as the LMP91000 potentiostat. It also does not fulfill the requirement of the op-amp LTC6268-10. Therefore towards the end of the discharge cycle, EIS and cyclic voltammetry cannot be performed. It also has the disadvantage of being much higher voltage for half of the discharge

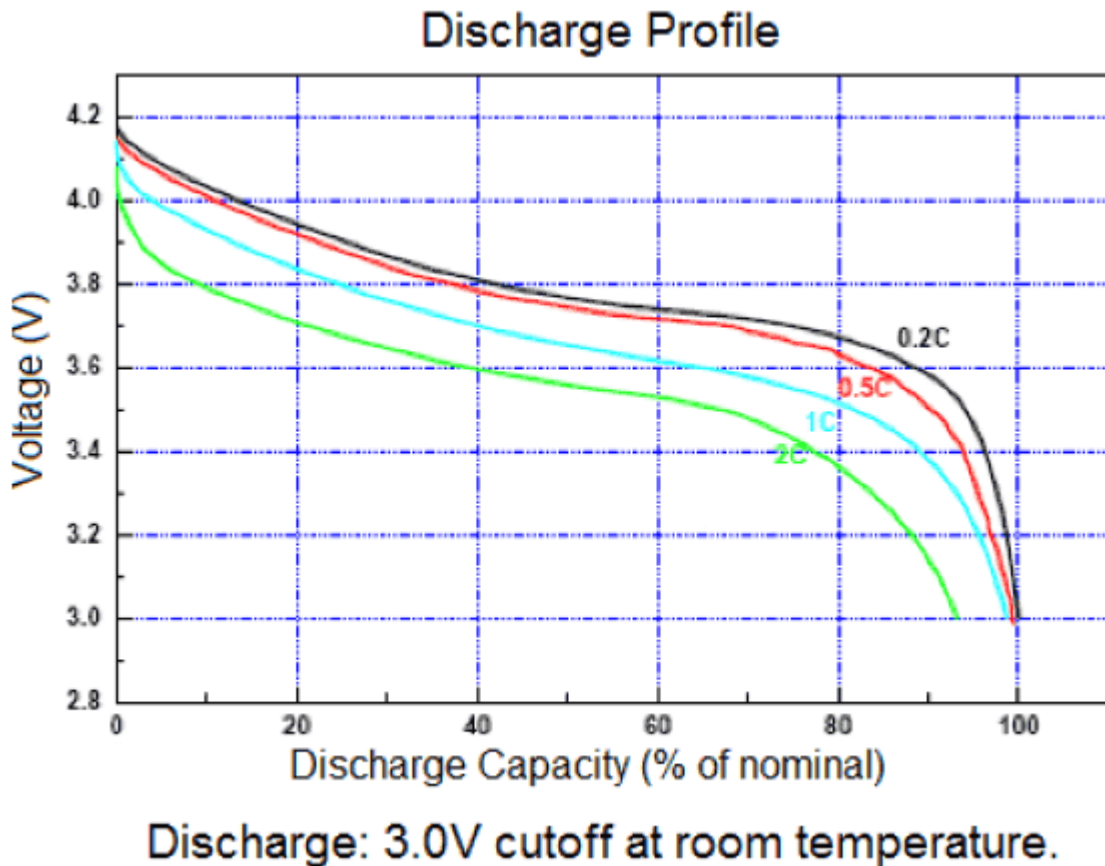


FIGURE 4.14: LiPo Discharge Graph[41]

cycle than the NiMH counterpart. This means that using LiPo will lead to higher losses in the LDO.

Hence, the decision is to use 3 NiMH batteries in series. The reason 4 cells are not used is because NiMH has a fully charged voltage of 1.4 to 1.5V depending on the cell. With 4 cells, this adds up to a maximum of 6V, which is the limit that the LDO can take. It is not desirable to operate exactly on the upper voltage limit of the LDO and hence only 3 cells are used. Additionally, charging circuitry which can charge batteries up to 6V typically needs a higher input voltage. This is not desirable at all as it means that the PCB must be turned off and disconnected from the batteries and charging circuit when in use, or to have a second LDO to handle the high input voltage.

Between the AAA and AA battery, the AA battery was chosen due to it being not much larger than the AAA battery but has almost twice the capacity. Although 1100mAh is estimated to be sufficient, a bigger battery will extend the usage time even further. In fact, with the 2000mAh battery, it is estimated that the PCB

Specs/Charger	LTC4060	BQ2002/F	DS2715	BQ24401
Fast Charge	Yes	Yes	Yes	Yes
Need MCU	No	No	No	No
Max Cells	4	4	10	NIL
Output Current (A)	0.4 - 2	NIL	NIL	Up to 2
Input Voltage (V)	4.5 - 10	4 - 6	4.5 - 16.5	4 - 6
Charge Time (Hours)	1 to 2.5	1 to 2.5	1 to 2.5	1 to 2.5
Quiscent current ( $\mu$ A)	<1	1	10	5

TABLE 4.13: Table of Battery Charging ICs

can last up to 20 days on a single charge. In addition, three AA batteries weigh in at 90g, which is still light enough for portable usage by a user who can simply slot the whole device into a pouch on the belt or in their pockets.

Finally, the batteries are arranged to be in 2 separate battery holders, one with one cell and the other with 2 cells. They will be connected in series as stated, but the purpose of this configuration is to be able to feed the voltage of the singular cell into an on-board ADC on the nRF52832 breakout board. This allows the MCU to monitor the battery voltage directly and can then trigger warnings to send to the user via Bluetooth when battery voltage is low (below 1.15V for example) and shut down when the battery voltage gets to 1.0V.

#### 4.2.10 Recharging IC

Since it has been determined that NiMH batteries are to be used, the next step is to find an IC that will handle the recharging of these batteries. Ideally, the charger should work with no input from the MCU. The reason for this is that if the batteries are completely depleted, the MCU will be in a shut down state and cannot interface with the charger IC. It is also desirable that the charger IC be able to work with a standard USB charger or at most up to 6V since that is what the LDO will take.

All of the above chargers will charge 3 NiMH cells without intervention from a MCU and all of them will charge the battery up in 2.5 hours or less and automatically stop charging when the batteries are full. All of them will also accept 5V inputs which allows for the use of common USB chargers. The main differentiating factor is the quiscent current draw from the battery once the DC adapter is disconnected. The best IC based on this is the LTC4060 with a draw of less than  $1\mu$ A.

The LTC4060 also has a feature of automatically stopping the charge if it detects that the battery has been removed or if the IC gets too hot. Additionally, it will automatically recharge any cells which discharge to 1.3V when the DC adapter is connected, and has 2 logic outputs which can drive an LED and be used as a logic signal to an MCU to let the MCU know that the batteries are being charged.

Hence, the decision is to use the LTC4060 with a USB charger, and for the power port on the PCB to be a micro-USB port.

Capabilities	mini-PCB
Communications	BLE to a smartphone, tablet or PC with MATLAB Data format is in ASCII which is easy to decode for any device
Measurements	Amperometry, Cyclic Voltammetry, EIS
Normal Operation	EIS twice per day Amperometry every half hour Cyclic Voltammetry only on demand
Amperometry	Any cell voltage from $\pm 0.792V$ Alternatively, if low power is not a concern, use the DAC and get $\pm 1.65V$
Cyclic Voltammetry	$-1.65V$ to $+1.65V$ in steps as small as $50\mu A$ if desired Typically set at 5mV steps Data captured at most at 860SPS
EIS	DC + 10Hz to 400kHz Alternatively, if low power not a concern, can go as low as 1Hz
Charge Time	2.5 Hours
Estimated Battery Life	20 Days

TABLE 4.14: Summary of PCB Capabilities

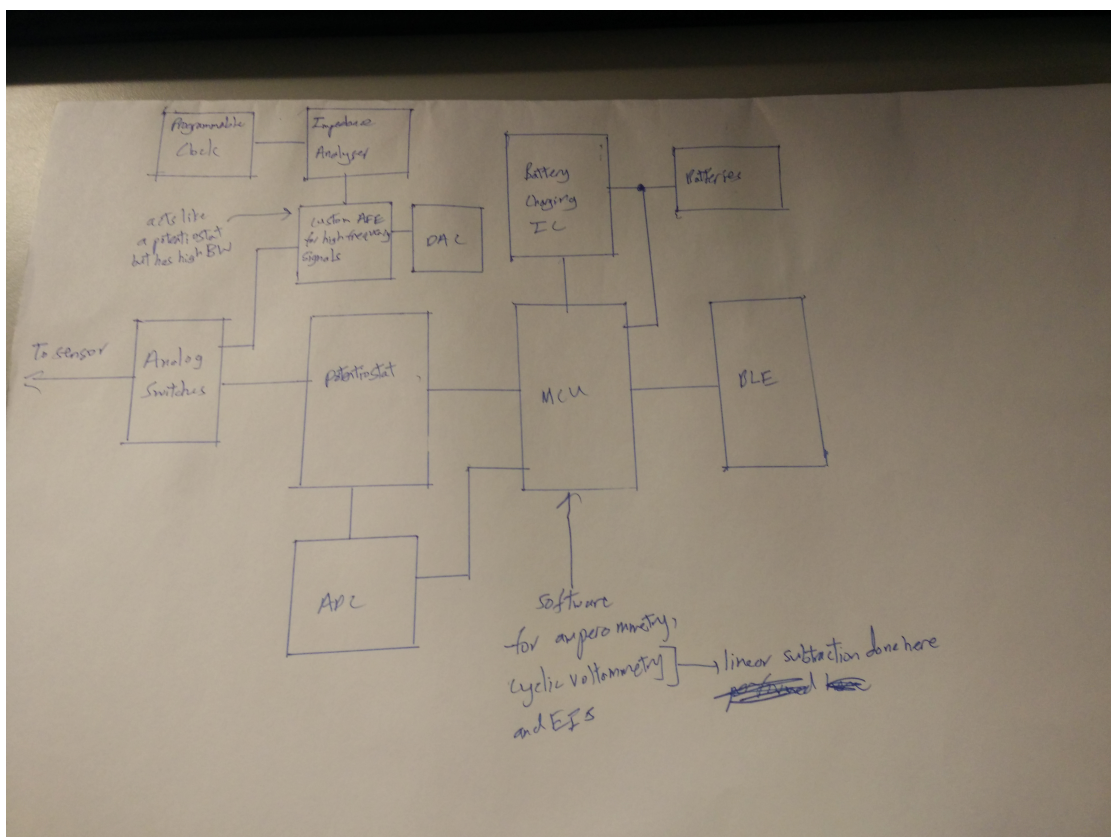


FIGURE 4.15: Final Block Diagram

### 4.2.11 Final Hardware Implementation

Table 4.14 summarises the main capabilities and features of the PCB.

The final hardware block diagram implementation is as shown below in Figure 4.15.



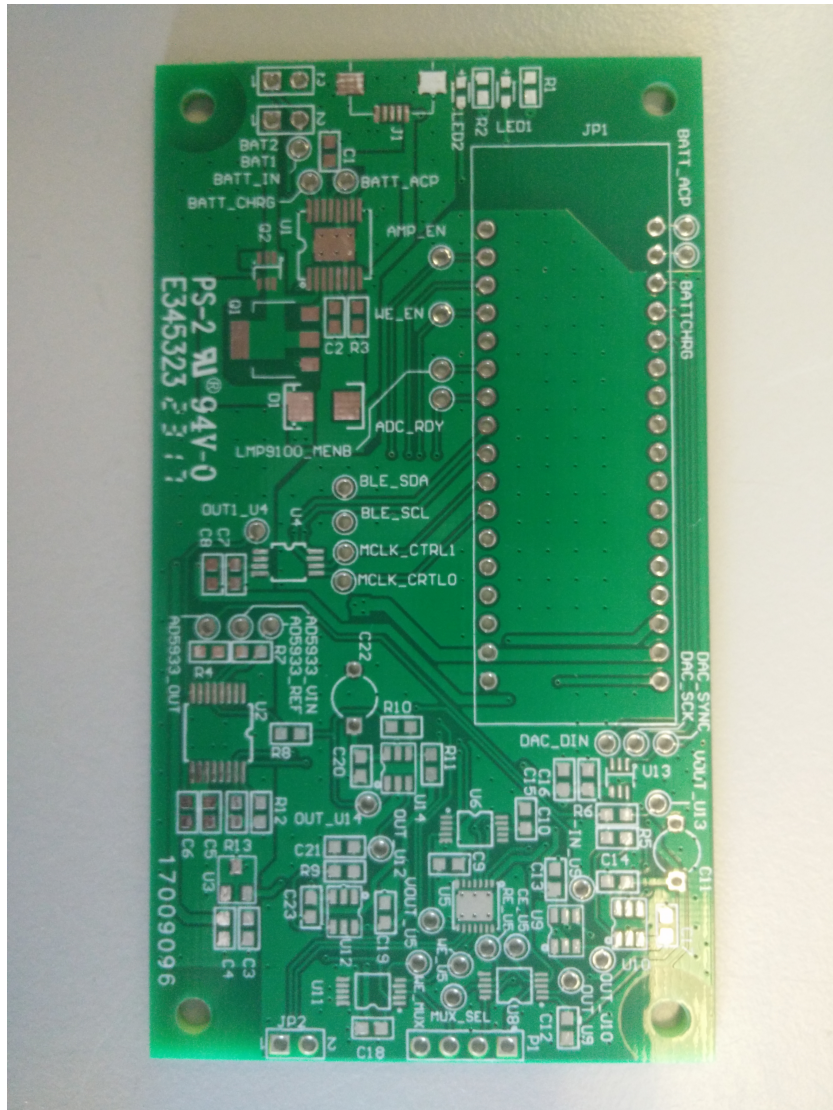


FIGURE 4.16: Bare PCB with no components on it

This circuit schematic was put into Altium Designer and then a 90mm x 50mm PCB developed. The exact schematic diagrams and PCB layout are attached in Appendix A, but pictures of the final PCB can be seen in Figures 4.16, 4.17 and 4.18.

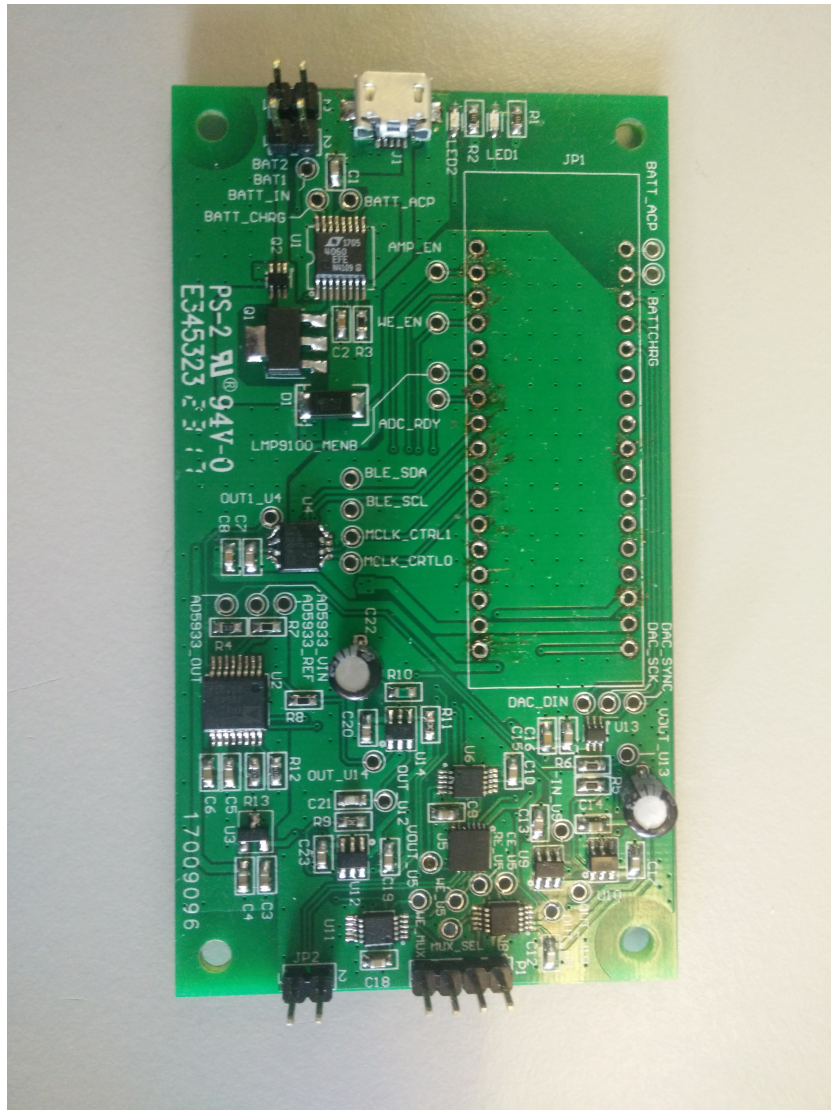


FIGURE 4.17: PCB with the parts soldered on

## 4.3 Software

### 4.3.1 Software on the MCU

The software is developed in the Arduino IDE as shown in Figures 4.19 and 4.20. The reason for this is that there are software cores and libraries which have been made publicly available[42][43] by that allow for the programming of generic nRF52832 devices and also uses the bluetooth stack developed by Nordic. In this way, the communication protocol is already implemented and saves a lot of time on debugging the BLE. It is also useful because it allows for serial communication with the nRF52832 which makes debugging easier.



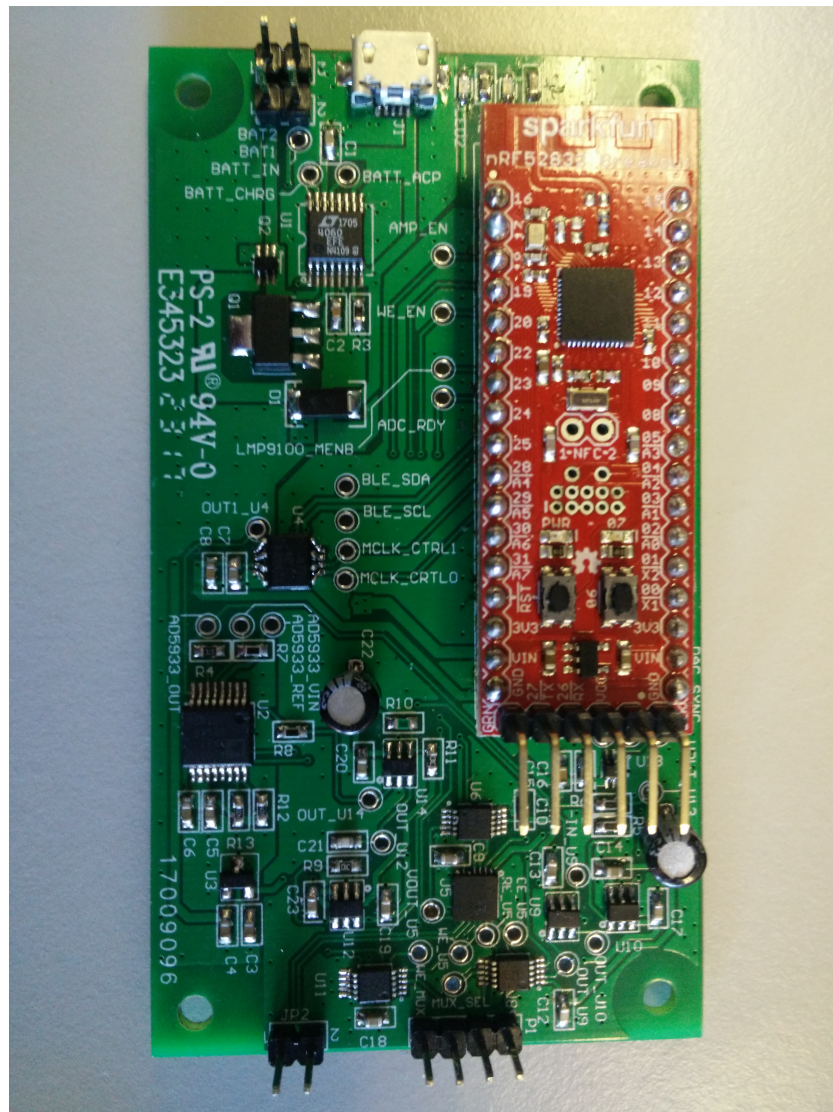


FIGURE 4.18: Complete PCB with Sparkfun breakout board

The core program is set to initialise all components of the PCB and to just hold for half an hour while the sensor stabilises. After half an hour, the sensor reading is obtained and if 2 consecutive readings 1 minute apart are within a certain tolerance, the sensor is assumed to have stabilised. Otherwise, the device goes to sleep for another 10 minutes and checks again. Repeat until the sensor is finally stable. If after 6 tries the sensor is still not stable, an alert is sent to the user to replace the sensor. Currently, the cell voltage is set to be approximately the same as that in Zhang's thesis, which is 0.528V. However, this voltage can be changed with a Bluetooth command from the smartphone. A full list of possible commands are shown in Table 4.15.

The commands in the table are what will be sent by the smartphone, tablet or

```

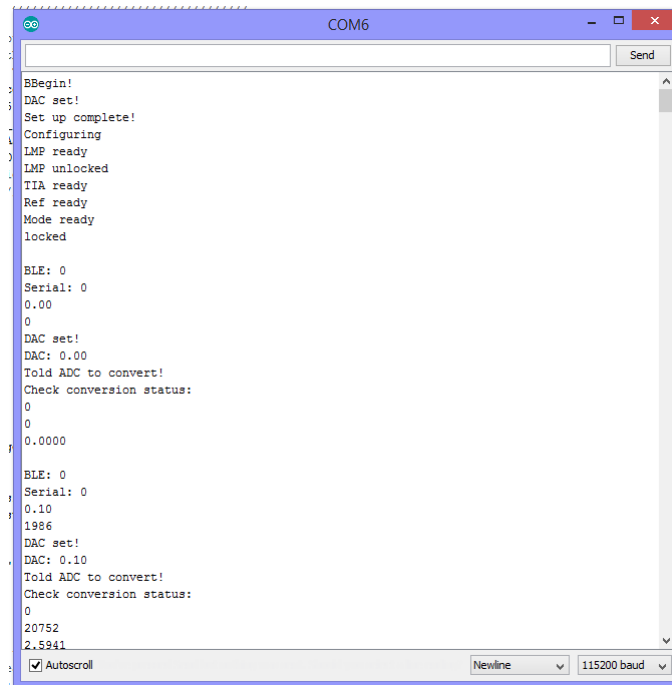
DAC_ADC_BLE | DAC_ADC_BLE | DAC_ADC_BLE
10 * service discoverable all UUIDs are MUI (Nordic UART Service) compatible.
11 *
12 * Please note that TX and RX characteristics use Notify and WriteWithoutResponse, so there's no guarantee
13 * that the data will make it to the other end. However, under normal circumstances and reasonable signal
14 * strength everything works well.
15 */
16
17
18 // Import libraries (BLEPeripheral depends on SPI)
19 #include <SPI.h>
20 #include <Wire.h>
21 #include <BLEPeripheral.h>
22 #include <BLESerial.h>
23
24 //Define all output pins from nRF52832 except I2C (which are defined in header file)
25 #define MUX_SEL 16
26 #define AMP_EN 17
27 #define WQ_MUX 18
28 #define WQ_EN 19
29 #define MENS 22
30 #define ALERT 23
31 #define CTRL0 28
32 #define CTRL1 29
33 #define BATT_ADC 15
34 #define BATT_CHRS 14
35 #define DAC_SYNC 13
36 #define SPI_SCK 12
37 #define MOSI 11
38 #define BATT_IN 5
39
40 //Custom boards may override default pin definitions with BLESerial(PIN_REQ, PIN_RDY, PIN_RST)
41 BLESerial bleSerial;
42
43 void setup() {
44 // custom services and characteristics can be added as well
45 bleSerial.setLocalName("BLE ADC DAC");
46
47 Serial.begin(115200);
48 bleSerial.begin();
49 Serial.println("Begin");
50
51 //DAC Setup////////////////////////////////////
52 pinMode(DAC_SYNC, OUTPUT);
53 pinMode(MOSI, OUTPUT);
54 pinMode(SPI_SCK, OUTPUT);
55
56

```

FIGURE 4.19: Arduino IDE

Commands	Replace all {number} with actual digits
d{number}	Reprograms the offset voltage that will be given by the DAC in EIS
c{number}	Start Cyclic Voltammetry with a peak expected at {number} volts Cyclic Voltammetry will take place over a 1V range
p{number}	Sets potentiostat cell voltage in amperometry
e	Perform EIS on demand. d{number} should be called beforehand if default offset voltage is not suitable
a	Get an amperometry reading on demand
b	Get battery voltage level

TABLE 4.15: Table of BLE commands



```
BBegin!  
DAC set!  
Set up complete!  
Configuring  
LMP ready  
LMP unlocked  
TIA ready  
Ref ready  
Mode ready  
locked  
  
BLE: 0  
Serial: 0  
0.00  
0  
DAC set!  
DAC: 0.00  
Told ADC to convert!  
Check conversion status:  
0  
0  
0.0000  
  
BLE: 0  
Serial: 0  
0.10  
1986  
DAC set!  
DAC: 0.10  
Told ADC to convert!  
Check conversion status:  
0  
20752  
2.5941
```

FIGURE 4.20: Serial Communication tool to aid in debugging

PC encoded as an ASCII string to the PCB. All Bluetooth communications are automatically stored into a buffer to be read by the main program. The main program calls a poll function to retrieve the communications and then process any data received. The data is read out 16 bits at a time and decoded. In Figure 4.21 for example, if a 'd' is the first ASCII character received, it is assumed that what follows is numbers that indicate the desired value. This is a reasonable assumption to make as in this project, we have full control over both the PCB and the receiving device. So if an app or MATLAB code were to be written, it should be written in such a way that the sent data is always formatted correctly. Furthermore, there are only a few commands possible, so it should be reasonable to ensure that there is correct formatting. By making this assumption, we save a little power in reducing the amount of conditional branches to take in the code and instructions to execute.

The main loop in the code is shown in Figure 4.22. The loop first checks if it has been too long since the last EIS. Since the PCB always sleeps for fixed intervals, it is possible to estimate when half a day has passed based on how many times the loop has been repeated. Next, it checks the Bluetooth for any incoming communication. The *forward()* function implements all the functions described in the previous table in the event of incoming commands. Note that currently the loop does not have the right amount of cycles to make up half an hour. In

```
void forward() {
  int bytecount = 0;
  int phonecount = 0;
  if (bleSerial && Serial) {
    int byte;
    char phonemessage;
    if((byte = bleSerial.read()) > 0){
      phonemessage = (char)byte;
      Serial.write(phonemessage);
      //if key character is sent to change DAC levels
      if(phonemessage == 'd' || byte == 'D'){
        Serial.println("got here");
        String fullmessage;
        float dacvoltage;
        while ((byte = bleSerial.read()) > 0){
          phonemessage = (char)byte;
          fullmessage += phonemessage;
        }
        dacvoltage = fullmessage.toFloat();
        dacwrite(dacvoltage);
      }
    }
  }
}
```

FIGURE 4.21: BLE Polling

the interest of testing, the period has been greatly shortened. This can be easily changed once the PCB is ready to be deployed. If the PCB is pre-programmed to work correctly with a given sensor and this communication is unnecessary (i.e the PCB is purely a transmitter and the smartphone/tablet/PC is purely a receiver of data), the PCB can be put into sleep mode for half an hour and this loop can be removed. This will reduce the power consumption of the board even further. The reason is that the user will not need to reprogram anything, and under normal operation, an amperometry reading every half an hour is sufficient. The only useful capability that is lost is the ability to check battery levels on demand.

After sufficient time has passed, we obtain a normal amperometric reading, send it out and repeat the loop again.

In the case of cyclic voltammetry, the background subtraction algorithm is implemented in software, where a linear approximation is made by taking current levels at  $\pm 0.1V$  and fitting a straight line through them.

```
int timesincecalibration = 0;
int keeppolling = 0;

void loop() {
  String adcreult;
  int battvoltage = 0;
  float battfloat = 0;

  timesincecalibration++;
  if (timesincecalibration == 24)
  {
    eiscalibrate();
    timesincecalibration = 0;
  }

  while (keeppolling < 1) {
    bleSerial.poll();
    keeppolling++;
    forward();
    lowpower.sleep((unsigned long)10000);//Sleep for 10 seconds
  }

  keeppolling = 0;

  adcreult = String(adc_single_convert(), 6); //Get amperometry reading
  bleSerial.println(adcreult);

  dacvoltage = dacvoltage + 0.1;
  battvoltage = analogRead(BATT_IN);
  Serial.print("Battery: ");
  Serial.println(battvoltage);
  battfloat = battvoltage;
  battfloat = battfloat/16383 * 3.3;
  Serial.println(battfloat, 4);
  // Transmit low battery warning if voltage levels dip to 1.1 and below
  if(battvoltage <= 5461) //5461 = 1.1V in 14bits with 3.3V as full scale
  {
    bleSerial.write("LOW BATTERY");
  }

  //Currently still in development
  lowpower.sleep((unsigned long)10000);//Sleep for 10 seconds
}
```

FIGURE 4.22: Main Loop in Code

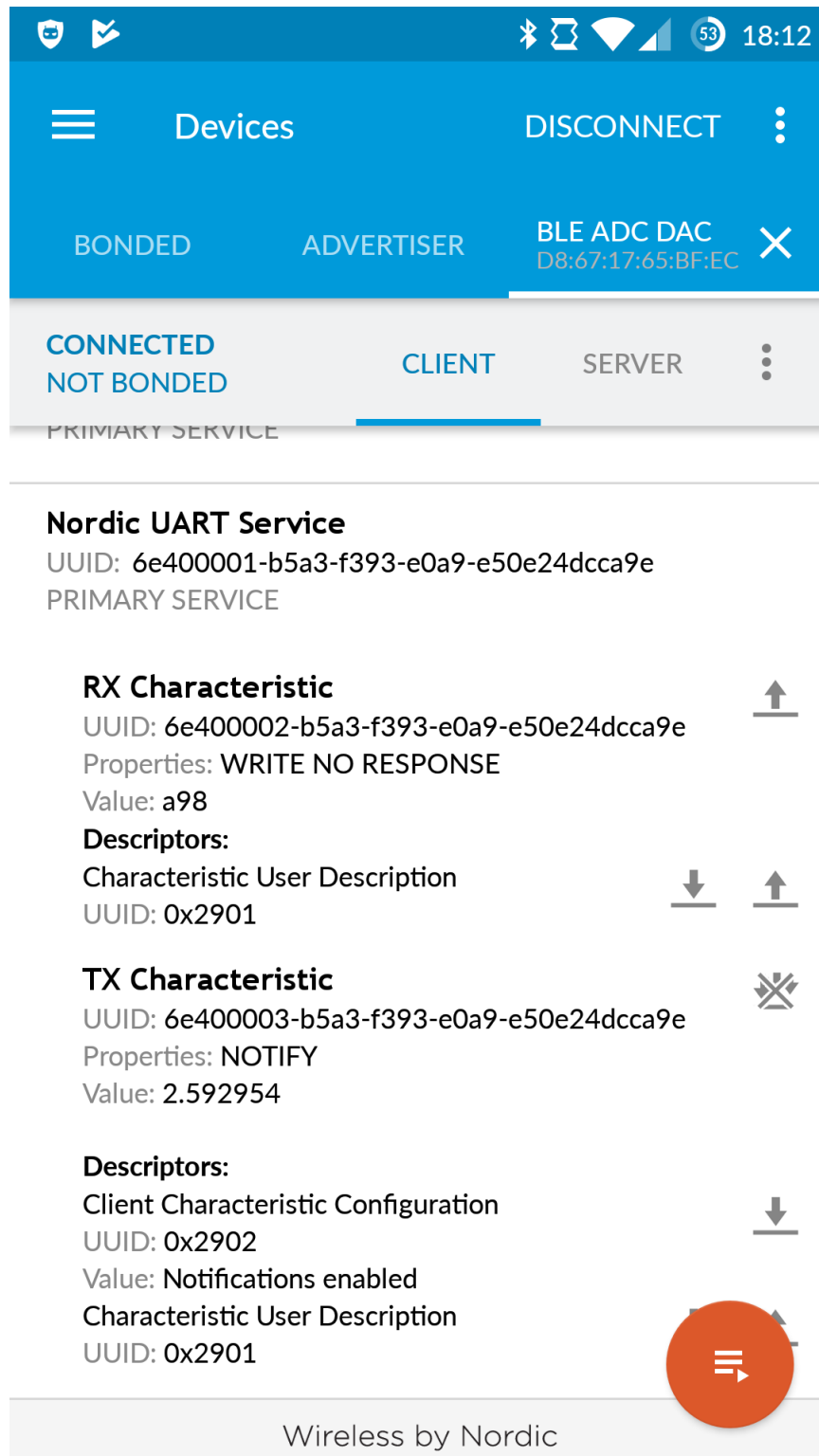


FIGURE 4.23: NiMH Discharge Graph



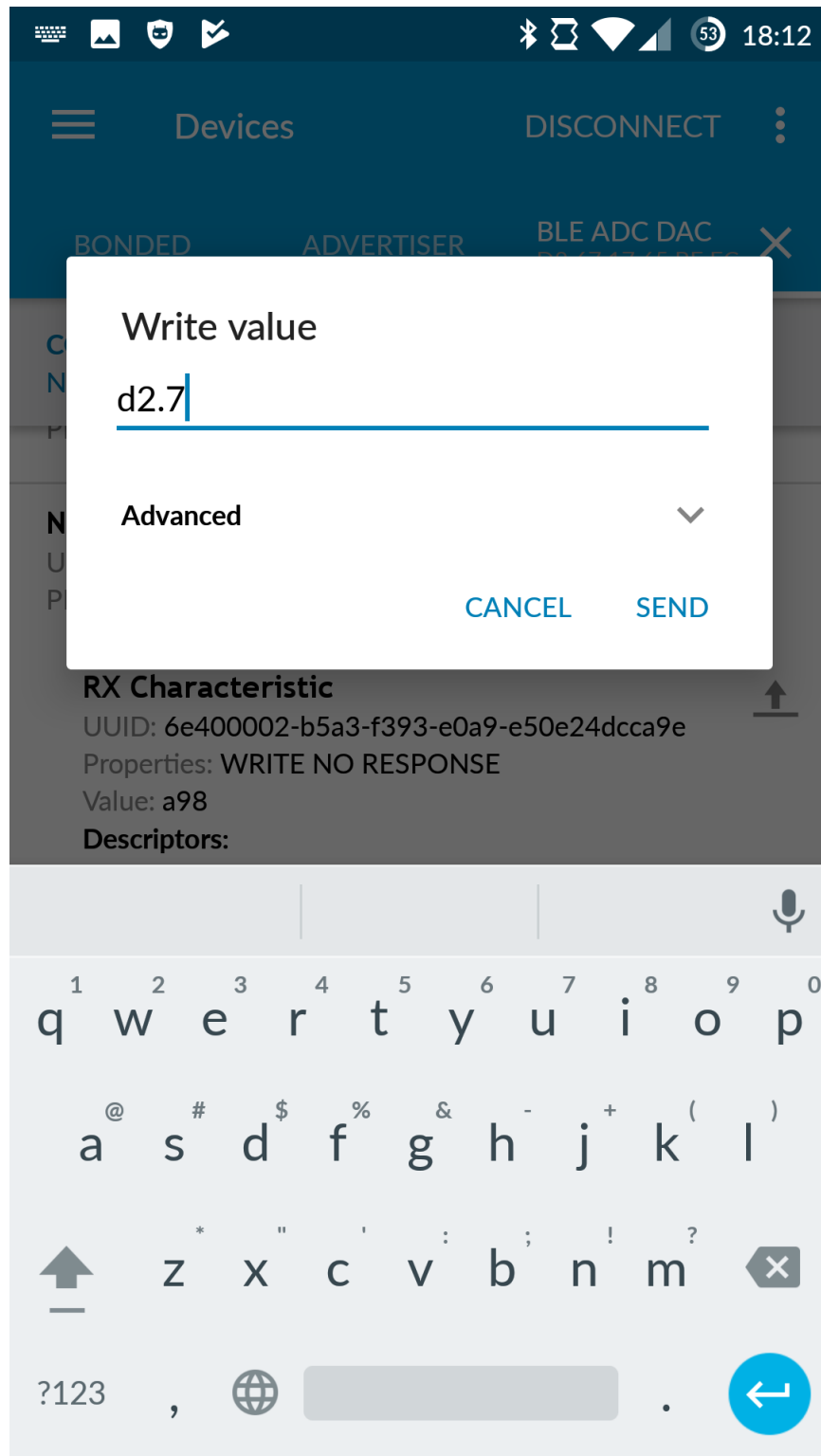


FIGURE 4.24: NiMH Discharge Graph



FIGURE 4.25: Screenshot of nRF Logger

### 4.3.2 Receiving End Software

The communications to and from the PCB were tested with Android Apps developed by Nordic Semiconductor. They are called nRF Connect as seen in Figures 4.23 and 4.24 and nRF Logger as in Figure 4.25. nRF Connect allows for serial communication with the PCB. The user is able to input an ASCII string using the phone and send it to the PCB. Conversely, the PCB will encode any data into ASCII strings and send them back to the phone. At the end of a session, nRF Connect will save the communications into a log file which is then viewable in nRF Logger.

An alternative form of communication is to get a BLE-enabled computer and run MATLAB. This environment will be preferred by users who want to perform complex processing on the data. MATLAB natively supports ASCII encoded messages as well as binary data, which means that no modification to the program on the PCB needs to be done in order to work with MATLAB.

# Chapter 5

## Evaluation and Conclusion

### 5.1 Evaluation

The testing is done on a prototype version of the PCB as shown in Figures 5.1 and 5.2. The power supply comes directly through USB from the PC into the LDO instead of batteries, which means that the supply rails will be much noisier than usual. Unfortunately, tests were run on dummy loads comprising of resistors. The reason for this is that the electrochemical sensor which was provided is only rated to last up to 14 days. By the time testing on the prototype began, the sensor had already been opened from its packaging for almost 3 months and had degraded. Testing it with the bench instrument yielded abnormal readings in the range of microamps and the sensor is unresponsive to glucose changes. An alternative sensor was provided as shown in Figure 5.3. However, this sensor was too noisy to be reliably compared against as can be seen from the readings in Figure 5.4. The steps are glucose concentrations of 2.5mM, 5mM and 7.5mM in that order. It can be seen that it is difficult to reliably distinguish 5mM and 7.5mM as their range of readings overlap. Therefore, in the absence of time, dummy loads were used instead. In this case, CE and RE are shorted together to close the feedback loop and a resistor was inserted across RE and WE. The TIA is configured to have a gain of 350,000.

First, cyclic voltammetry was done using a 560k $\Omega$  resistor. The DAC was swept from 0V to 3.3V and the TIA in the LMP91000 was set to have its internal zero about 1.65V. Therefore, this is equivalent to a cyclic voltammetry sweep of -1.65V to 1.65V. The backwards sweep was not performed since it can be expected that

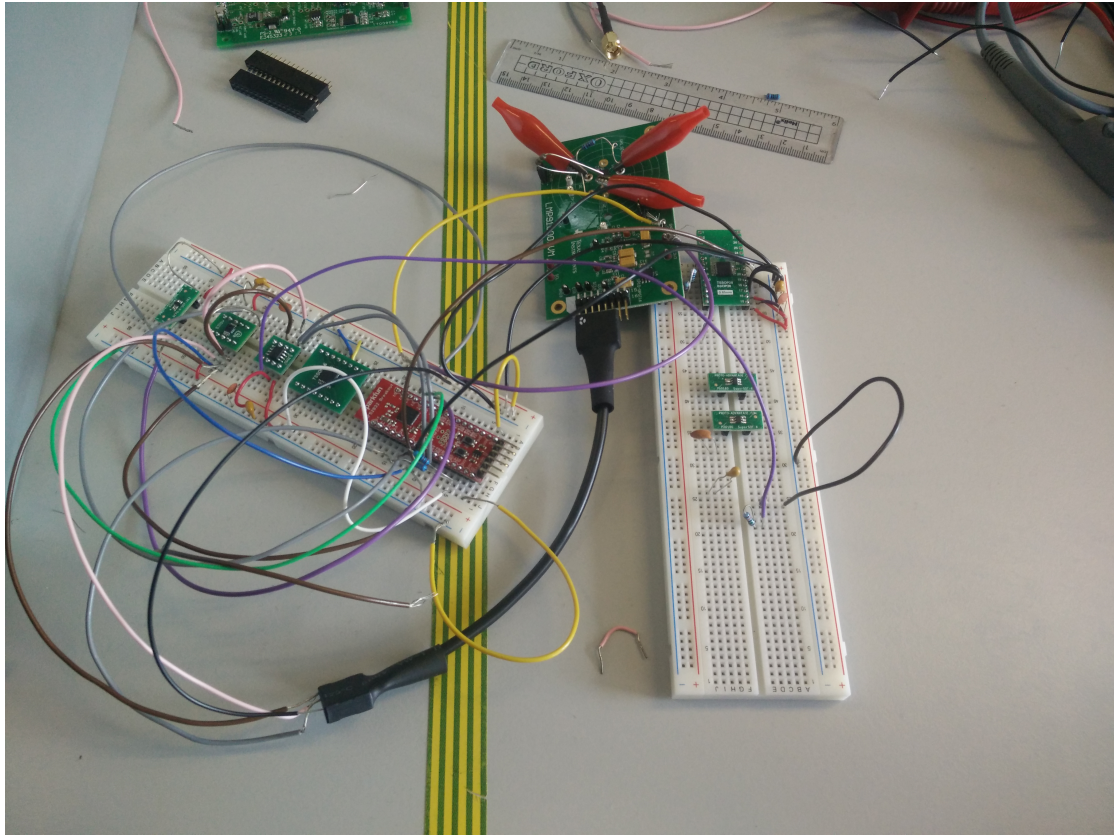


FIGURE 5.1: Picture of Prototype

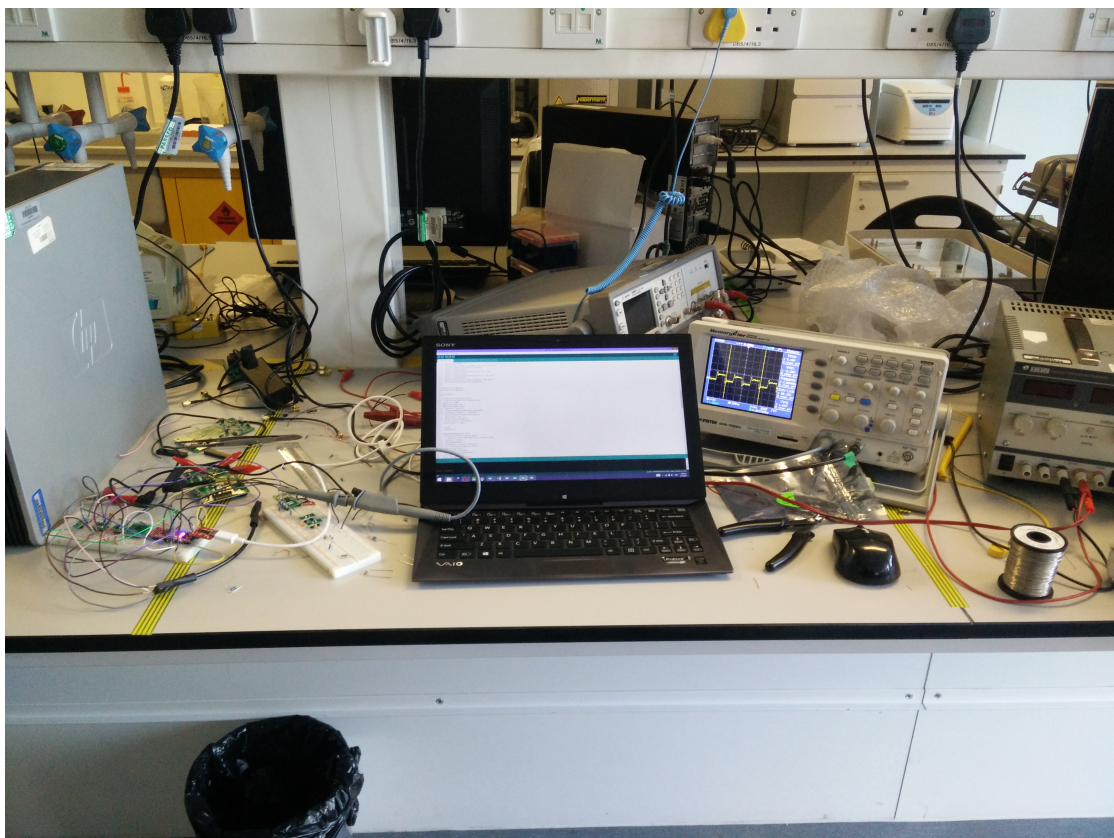


FIGURE 5.2: Picture of prototype with PC, oscilloscope and power supply



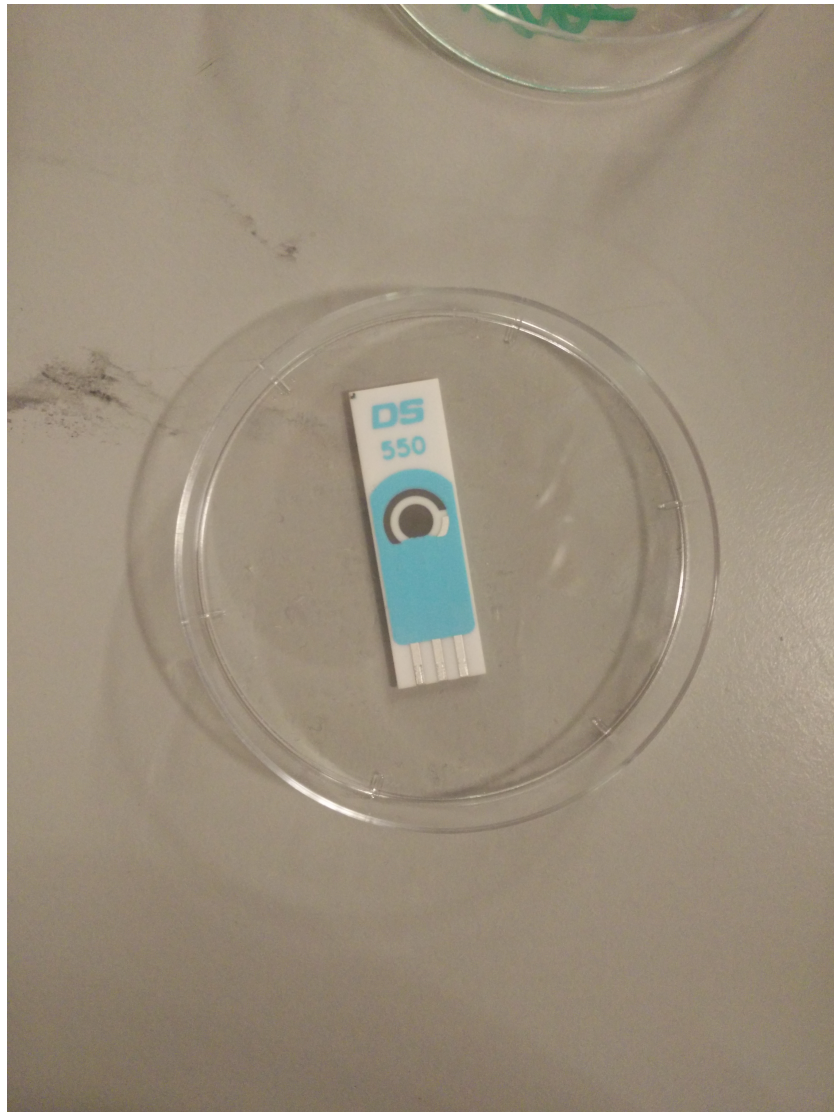


FIGURE 5.3: Picture of new glucose sensor

there will not be any difference when it is a resistor. The graph extracted is as shown in Figure 5.5.

The results are indeed as expected, with a fairly linear relationship between the output of the TIA and the input voltage. It is not perfect however, as the slope is slightly different on the left of approximately 1.2V compared to the right. On the left, the slope is approximately -0.04V per 0.1V increase in DAC output. On the right, it becomes approximately -0.07V per 0.1V increase in DAC output. This measurement was repeated with similar results. It is also noted that there is an offset in the results, as when 1.65V was output (and verified with an oscilloscope), the output of the TIA is at 1.70V instead of 1.65. This translates to an offset of



FIGURE 5.4: Readings from new sensor

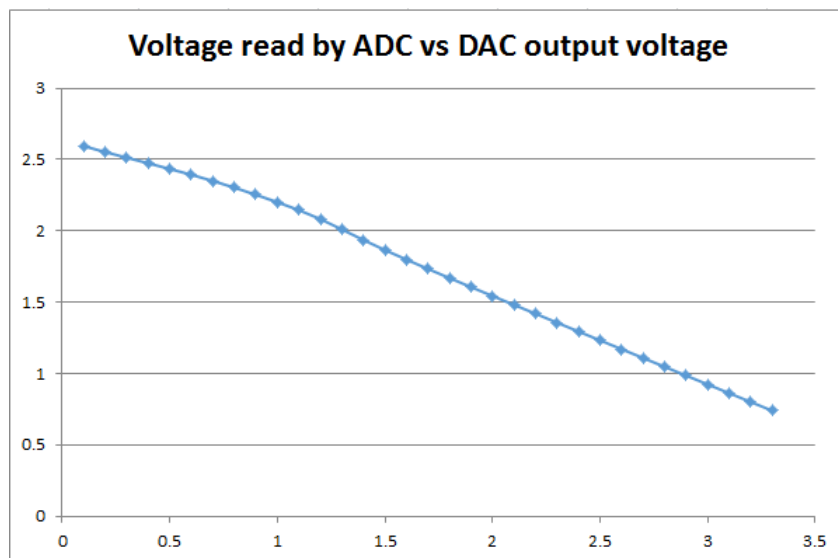


FIGURE 5.5: Readings from Cyclic Voltammetry

0.5V which translates to an offset of about 200nA. This offset could be the reason why the slope is different on both sides.

Amperometry is done on a variety of resistor values with different TIA gains. Excluding the last result, the errors are all within 9%, going as low as 0.3%. It should also be noted at this point that the testing environment is extremely noisy, with the oscilloscope trace having tens of millivolts of noise. This could be due to the long wires in the prototype coupling noise. The actual PCB should be expected to have less due to the absence of wires.

Vcell	Resistor	Expected Current	Vout(Scope)	Vout(ADC)	Gain	Actual Current	Internal zero	disconnected RE and WE, Vout=1.70V
0.528	10000000	5.28E-08	1.72	1.72	350000	5.71429E-08	1.65	
0.792	10000000	7.92E-08	1.73	1.73	350000	8.57143E-08	1.65	
0.792	4700000	1.68511E-07	1.76	1.76	350000	1.71429E-07	1.65	
0.792	1200000	0.00000066	1.95	1.95	350000	7.14286E-07	1.65	
0.528	560000	9.42857E-07	1.03	1.03	350000	0.00000094	0.66	disconnected RE and WE, Vout = 701mV
0.528	150000	0.00000352	1.94	1.94	350000	0.00000354	0.66	
0.528	56000	9.42857E-06	1.84	1.84	120000	9.49167E-06	0.66	
0.528	10000	0.0000528	2.47	2.47	35000	5.05429E-05	0.66	
0.528	5600	9.42857E-05	1.36	1.36	7000	9.41429E-05	0.66	
0.528	1000	0.000528	2.9	2.9	7000	0.000314143	0.66	

FIGURE 5.6: Readings from Amperometry

Finally, EIS is performed. The EIS sweep below 100Hz is found to be extremely slow, especially at 30Hz and below (a few minutes per reading). At 1 to 9Hz, each reading takes tens of minutes to complete, which makes it impractical in terms of both time taken and the impact on battery life. Therefore, the EIS was conducted to only 10Hz. The upper limit was set to be 400kHz.

Analog Devices recommend that calibration be carried out on the AD5933 using a resistive load which is one-third of the range between minimum expected impedance and maximum expected impedance. In this case, it is 700 $\Omega$ . However, the closest resistor value that was available was 660 $\Omega$ , therefore that was used. After calibration, EIS was then performed with 220 $\Omega$ , 1.8k $\Omega$  and the original 660 $\Omega$  resistor.

It can be seen from Figure ?? that while it is very accurate for the calibration resistor, there exists a constant offset for the other 2 resistors, continually overestimating the 220 $\Omega$  resistor and underestimating the 1.8k $\Omega$  resistor. Such offsets can be corrected for in the MCU when the results are collected. In terms of variation, the variation on the calibration resistor is less than 0.2%. The variation on both the 220 $\Omega$  and 1.8k $\Omega$  is just over 1%. There is no phase variation or error throughout the range, with phase being correctly reported as zero.

## 5.2 Future Work

Beyond this report, the actual PCB will be tested with a new sensor similar to the type shown in Figure 5.3 which is less prone to noise. The findings will then be detailed in the presentation in place of the results from the dummy resistors. EIS should also be investigated on the actual PCB and correction algorithms put in place to account for such offsets.



Freq	660	Phase	220	Phase	1800	Phase
400000	660.18	0	228.2	0	1689.56	0
300000	660.23	0	228.79	0	1693.69	0
200000	659.96	0	229.06	0	1703.1	0
100000	660.23	0	229.21	0	1702.86	0
90000	660	0	227.59	0	1707.5	0
80000	659.92	0	227.93	0	1703.4	0
70000	660.34	0	228.9	0	1711.6	0
60000	660	0	228	0	1708.2	0
50000	660.6	0	227.9	0	1709.5	0
40000	659.9	0	228.1	0	1707.69	0
30000	660	0	228.13	0	1706.8	0
20000	660.2	0	227.98	0	1704.1	0
10000	660	0	228	0	1712.6	0
9000	660	0	227.59	0	1695.32	0
8000	660.3	0	228	0	1703.64	0
7000	659.8	0	228.93	0	1700.3	0
6000	660.1	0	228.56	0	1702	0
5000	660	0	228.32	0	1699.54	0
4000	660	0	228.45	0	1706.9	0
3000	660.12	0	228.37	0	1694.6	0
2000	659.9	0	227.69	0	1708.9	0
1000	659.9	0	228	0	1707.3	0
900	659.8	0	227.58	0	1702.8	0
800	659.75	0	229	0	1688.12	0
700	660	0	229.65	0	1695.36	0
600	660.25	0	229.42	0	1695.25	0
500	660.41	0	229.31	0	1702.3	0
400	660.52	0	229	0	1700.56	0
300	660	0	228.19	0	1701.5	0
200	659.89	0	228	0	1701.94	0
100	660.01	0	228	0	1703.3	0
90	660.05	0	227.99	0	1703.3	0
80	660	0	228.56	0	1704.42	0
70	659.98	0	228.46	0	1699.8	0
60	659.88	0	229	0	1697.53	0
50	660.45	0	229.1	0	1710.2	0
40	660.35	0	229.05	0	1709.88	0
30	660.03	0	228	0	1702.4	0
20	660	0	228.78	0	1701.5	0
10	660	0	228.95	0	1701	0

FIGURE 5.7: Readings from EIS

## 5.3 Conclusion

To conclude, this report summarises and highlights the work that has been carried out by myself with guidance from my supervisor Dr Sara S. Ghoreishizadeh. The purpose and medical motivation for this project was discussed, with the literature review being focused on the main part of this project which is background subtraction. Various methods such as analog background subtraction, analog filtering, offset compensate, linear estimation and polynomial fitting were discussed and the merits and drawbacks of each presented. After weighing the pros and cons, the last two methods were deemed suitable and worth taking forward beyond this interim report.

An overall hardware schematic was also presented with several hardware components such as the potentiostat AFE and impedance measurement circuit discussed and potential ICs chosen. A custom AFE to interface the impedance analyzer was also discussed and implemented.

Finally, a PCB was successfully designed and the prototype of which was tested with dummy resistors.

The results of the prototype are actually fairly promising, especially when considering that it was tested in an extremely noisy environment. Most of the major errors are from deterministic offsets and can be corrected with software algorithm changes.

All in all, a PCB that is capable of lasting 20 days on a single charge, can perform chronoamperometry, EIS and cyclic voltammetry was successfully designed and made throughout the course of this final year project.

# Appendix A

## Altium Schematic and PCB layout

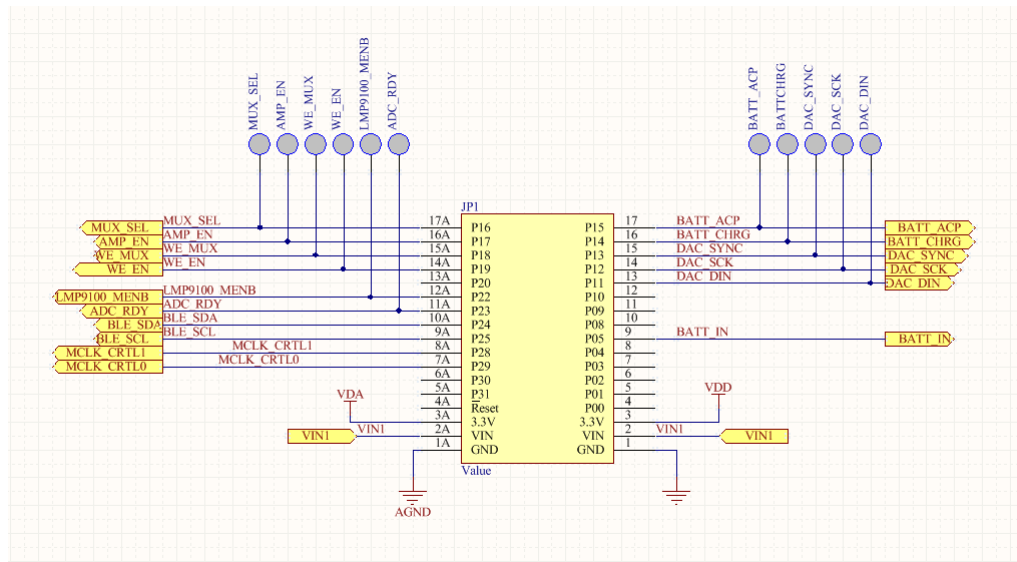


FIGURE A.1: Schematic of connections to nRF52832 breakout

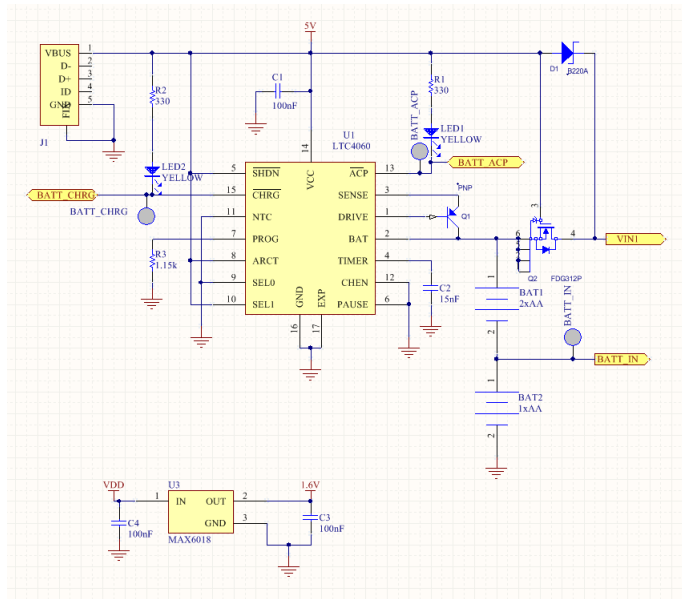


FIGURE A.2: Schematic of Battery Charger

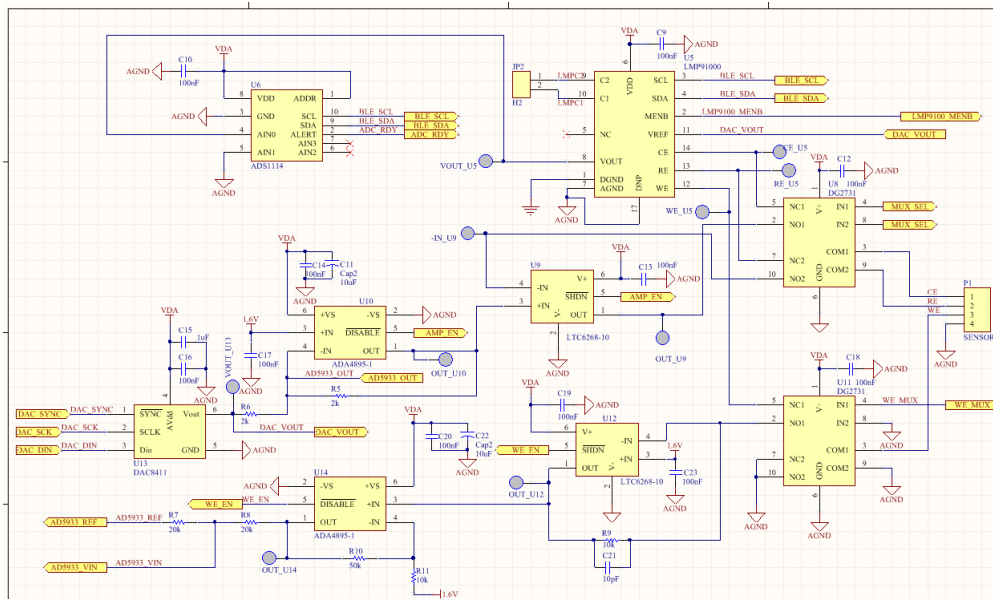


FIGURE A.3: Schematic of custom AFE



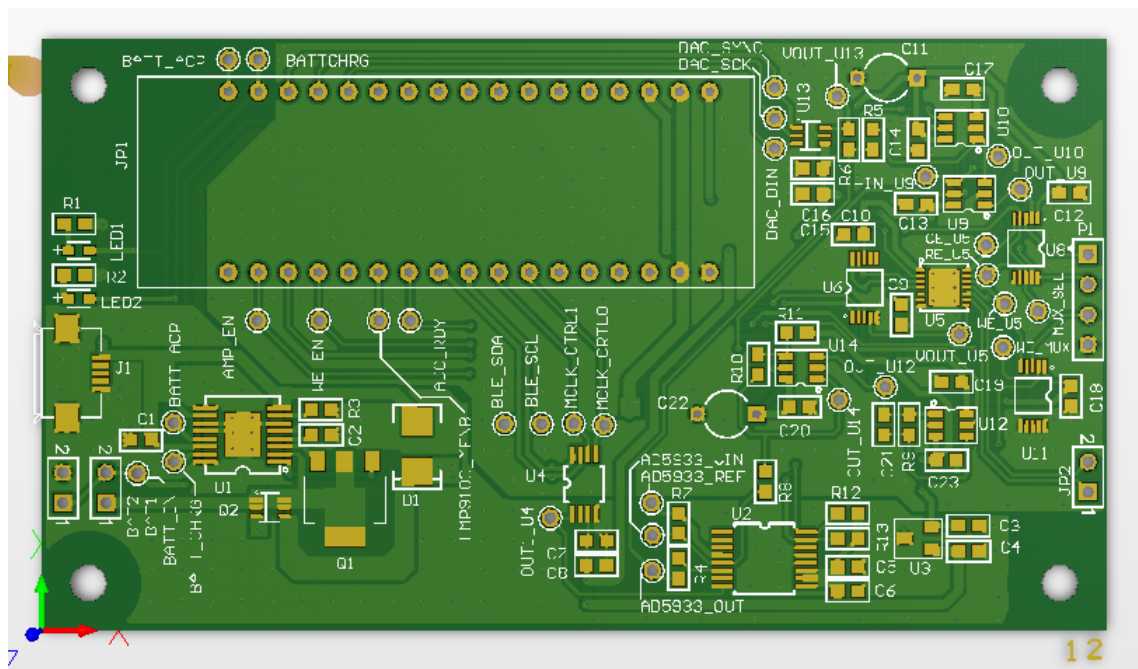


FIGURE A.6: 3D view of PCB

# Bibliography

- [1] Giovanni De Micheli et al. “An Integrated Platform for Advanced Diagnostics”. In: Design, Automation & Test in Europe Conference & Exhibition (DATE). Mar. 2011. DOI: 10.1109/DATE.2011.5763235.
- [2] A.L. Galant, R.C. Kaufman, and J.D. Wilson. “Glucose: Detection and analysis”. In: *Food Chemistry* 188 (Dec. 2015), pp. 149–160. DOI: 10.1016/j.foodchem.2015.04.071.
- [3] Shurui Cao et al. “An integrated sensing system for detection of cholesterol based on TiO<sub>2</sub>–graphene–Pt–Pd hybridnanocomposites”. In: *Biosensors and Bioelectronics* 42 (Apr. 2013), pp. 532–538. DOI: 10.1016/j.bios.2012.10.048.
- [4] Marcelo Ricardo Romero et al. “Amperometric Biosensor for Direct Blood Lactate Detection”. In: *Analytical Chemistry* 83 (13) (2010), pp. 5568–5572. DOI: 10.1021/ac1004426.
- [5] Mamun Jamal et al. “Disposable sensor based on enzyme-free Ni nanowire array electrode to detect glutamate”. In: *Biosensors and Bioelectronics* 40 (1) (Feb. 2013), pp. 213–218. DOI: 10.1016/j.bios.2012.07.024.
- [6] Allen J. Bard and Larry R. Faulkner. *Electrochemical Methods: Fundamentals and Applications*. John Wiley & Sons, 2001. ISBN: 978-0471043720.
- [7] John D Isaacs and Gianfranco Ferraccioli. “The need for personalised medicine for rheumatoid arthritis”. In: *Annals of the Rheumatic Diseases* 70 (1) (2011), pp. 4–7. DOI: 10.1136/ard.2010.135376.
- [8] Xiaotian Zhang. “Study of Glucose sensor’s sensitivity and impedance over time and an embedded system for their real-time measurement”. thesis. Imperial College London, Sept. 2016.

- [9] Andre Hermans et al. “Dopamine Detection with Fast-Scan Cyclic Voltammetry Used with Analog Background Subtraction”. In: *Analytical Chemistry* 80 (11) (Apr. 2008), pp. 4040–4048. DOI: 10.1109/TBCAS.2015.2421513.
- [10] Donita L. Robinson et al. “Detecting Subsecond Dopamine Release with Fast-Scan Cyclic Voltammetry in Vivo”. In: *Clinical Chemistry* 49 (10) (Oct. 2003), pp. 1763–1773. DOI: 10.1373/49.10.1763.
- [11] Michael AC, Borland LM, and editors. *Electrochemical Methods for Neuroscience*. Taylor Francis, 2006. Chap. 4. ISBN: 9780849340758.
- [12] Pantelis Georgiou. *EE3.21 Biomedical Electronics*. Imperial College London, 2015.
- [13] Daniel L. Purich. *Enzyme Kinetics: Catalysis & Control*. Elsevier, 2010. ISBN: 978-0-12-380924-7.
- [14] C.M. Wong, K.H. Wong, and X.D. Chen. “Glucose oxidase: natural occurrence, function, properties and industrial applications”. In: *Computer Vision and Image Understanding* 78 (6) (Mar. 2008), pp. 927–938. DOI: 10.1007/s00253-008-1407-4.
- [15] Sen-ching S. Cheung and Chandrika Kamatha. “Robust techniques for background subtraction in urban traffic video”. In: *SPIE Proceedings*. Vol. 5308. Jan. 2004. DOI: 10.1117/12.526886.
- [16] Andrews Sobrala and Antoine Vacavant. “A comprehensive review of background subtraction algorithms evaluated with synthetic and real videos”. In: *Computer Vision and Image Understanding* 122 (May 2014), pp. 4–21. DOI: 10.1016/j.cviu.2013.12.005.
- [17] Carlos I. Dorta-Quiñones et al. “A Wireless FSCV Monitoring IC With Analog Background Subtraction and UWB Telemetry”. In: *IEEE Transactions on Biomedical Circuits and Systems* 10 (2) (Apr. 2016), pp. 289–299. DOI: 10.1109/TBCAS.2015.2421513.
- [18] Jonathon O. Howell, Werner G. Kuhr, and R. Mark Wightman. “Background subtraction for rapid scan voltammetry”. In: *Journal of Electroanalytical Chemistry and Interfacial Electrochemistry* 209 (1) (Sept. 1986), pp. 77–90. DOI: 10.1016/0022-0728(86)80187-5.
- [19] Paula S. Cahill et al. “Microelectrodes for the Measurement of Catecholamines in Biological Systems”. In: *Analytical Chemistry* 68 (18) (Sept. 1996), pp. 3180–3186. DOI: 10.1021/ac960347d.



- [20] Barry H. Ginsberg. “Factors Affecting Blood Glucose Monitoring: Sources of Errors in Measurement”. In: *Journal of diabetes science and technology* 3, PMC2769960 (4) (Jul. 2009), pp. 903–913.
- [21] Lukasz Górski, Filip Ciepiela, and Małgorzata Jakubowska. “Automatic baseline correction in voltammetry”. In: *Electrochimica Acta* 136 (Aug. 2014), pp. 195–203. DOI: 10.1016/j.electacta.2014.05.076.
- [22] Sen-ching S. Cheung and Chandrika Kamatha. “Baseline correction by improved iterative polynomial fitting with automatic threshold”. In: International Conference on Chemometrics and Bioinformatics in Asia — CCBA 2004. Oct. 2004. DOI: 10.1016/j.chemolab.2005.08.009.
- [23] Konstantinos I. Papadimitriou et al. “Towards A High-Precision, Embedded System For Versatile Sensitive Biosensing Measurements”. In: *Biomedical Circuits and Systems Conference (BioCAS), 2015 IEEE*. Oct. 2015. DOI: 10.1109/BioCAS.2015.7348432.
- [24] Vijay Degalahal and Tim Tuan. “Methodology for High Level Estimation of FPGA Power Consumption”. In: ASP-DAC ’05 Proceedings of the 2005 Asia and South Pacific Design Automation Conference. (Jan. 2005, pp. 657–660. DOI: 10.1145/1120725.1120986.
- [25] Santhosh Kumar Rethinagiri et al. “Hybrid System Level Power Consumption Estimation for FPGA-Based MPSoC”. In: Computer Design (ICCD), 2011 IEEE 29th International Conference on. (Oct. 2011, pp. 239–246. DOI: 10.1109/ICCD.2011.6081403.
- [26] Juergen Becker, Michael Huebner, and Michael Ullmann. “Power Estimation and Power Measurement of Xilinx Virtex FPGAs: Trade-offs and Limitations”. In: Integrated Circuits and Systems Design, 2003. SBCCI 2003. Proceedings. 16th Symposium on. (Sep. 2003. DOI: 10.1109/SBCCI.2003.1232842.
- [27] Daniel Cardenas et al. “Fixed point and power consumption analysis of a coherent receiver for optical access networks implemented in FPGA”. In: Optical Communication (ECOC 2013), 39th European Conference and Exhibition on. (Oct. 2013. DOI: 10.1049/cp.2013.1283.
- [28] Abracon LLC. *Surface Mount WLAN / Bluetooth Chip Antenna (2450MHz)*. 2017. URL: <http://www.abracon.com/chip-antenna/AMCA31-2R450G-S1F-T.pdf>.

- [29] Pulse Electronics. *NFC Flex Stamp Antenna*. 2017. URL: <http://www.mouser.com/ds/2/336/-253143.pdf>.
- [30] Pulse Electronics. *2.4 GHz Helical WiFi SMD Antenna*. 2017. URL: <http://www.mouser.com/ds/2/336/-268286.pdf>.
- [31] Esko Strömmer, Mika Hillukkala, and Arto Ylisaukko-oja. “Ultra-low Power Sensors with Near Field Communication for Mobile Applications”. In: *IFIP International Federation for Information Processing* 248 (2007), pp. 132–142. DOI: 10.1007/978-0-387-74899-3\_12.
- [32] Carles Gomez, Joaquim Oller, and Josep Paradells. “Overview and Evaluation of Bluetooth Low Energy: An Emerging Low-Power Wireless Technology”. In: *Sensors* 12 (9) (Aug. 2012), pp. 11734–11753. DOI: 10.3390/s120911734.
- [33] Roy Friedman, Alex Kogan, and Yevgeny Krivolapov. “On Power and Throughput Tradeoffs of WiFi and Bluetooth in Smartphones”. In: *IEEE Transactions on Mobile Computing* 12 (7) (Jul. 2013), pp. 1363–1376. DOI: 10.1109/TMC.2012.117.
- [34] JDRF. *Continuous glucose monitors*. 2017. URL: <https://jdrf.org.uk/about-type-1-diabetes/treating/cgms/>.
- [35] Texas Instruments. *Bandwidth of LMP91000’s TIA*. 2015. URL: [https://e2e.ti.com/support/amplifiers/precision\\_amplifiers/f/14/t/469995](https://e2e.ti.com/support/amplifiers/precision_amplifiers/f/14/t/469995).
- [36] Munsters MJM and Saris WHM. “Effects of Meal Frequency on Metabolic Profiles and Substrate Partitioning in Lean Healthy Males”. In: *PLoS ONE* 7 (6) (Jun. 2012). DOI: 10.1371/journal.pone.0038632.
- [37] Konrad Chabowski et al. “Simple Wide Frequency Range Impedance Meter Based on AD5933 Integrated Circuit”. In: *Metrology and Measurement Systems* 22 (1) (Feb. 2015), pp. 13–24. DOI: 10.1515/mms-2015-0006.
- [38] P Bogónez-Franco et al. “Performance of an implantable impedance spectroscopy monitor using ZigBee”. In: *Journal of Physics: Conference Series* 224 (1) 2010). DOI: 10.1088/1742-6596/224/1/012163.
- [39] J. Ferreira, F. Seoane, and K. Lindecrantz. “AD5933-based electrical bioimpedance spectrometer. Towards textile-enabled applications”. In: *Engineering in Medicine and Biology Society, EMBC, 2011 Annual International Conference of the IEEE*. 2011. DOI: 10.1109/IEMBS.2011.6090891.

- 
- [40] Analog Devices. *Evaluating the AD5933 1 MSPS, 12-Bit Impedance Converter Network Analyzer*. 2012. URL: <http://www.analog.com/media/en/technical-documentation/evaluation-documentation/UG-364.pdf>.
- [41] Ktc. *Discharge Profile*. 2017. URL: <https://i.stack.imgur.com/LV91V.gif>.
- [42] sandeepmistry. *Arduino Core for Nordic Semiconductor nRF5 based boards*. 2017. URL: <https://github.com/sandeepmistry/arduino-nRF5>.
- [43] sandeepmistry. *An Arduino library for creating custom BLE peripherals with Nordic Semiconductor's nRF8001 or nR51822*. 2017. URL: <https://github.com/sandeepmistry/arduino-BLEPeripheral>.